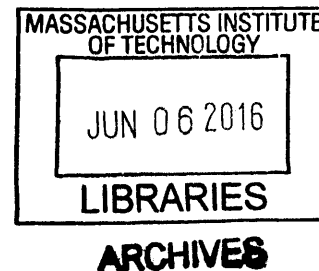# High Relaxivity Biomolecule Based Contrast Agents Engineered for Molecular Functional Magnetic Resonance Imaging

by
Vivian Hsieh

B.A.Sc. Chemical and Biological Engineering
University of British Columbia, 2008

M.S. Chemical Engineering Practice
Massachusetts Institute of Technology, 2011

Submitted to the Department of Chemical Engineering
in Partial Fulfillment of the Requirements for the Degree of

Doctor of Philosophy
at the
MASSACHUSETTS INSTITUTE OF TECHNOLOGY
June 2016

**Signature redacted**

Signature of Author ................................................................................
Department of Chemical Engineering
May 20, 2016

**Signature redacted**

Certified by ...........................................
Alan P. Jasanoff
Professor of Biological Engineering,
Brain and Cognitive Sciences, Nuclear Science and Engineering
Thesis Co-Supervisor

Certified by ...............................................................................
K. Dane Wittrup
Carbon P. Dubbs Professor of Chemical and Biological Engineering
Thesis Co-Supervisor

**Signature redacted**

Accepted by ...............................................
Richard D. Braatz
Edward R. Gilliland Professor of Chemical Engineering
Chairman, Committee for Graduate Students

# High Relaxivity Biomolecule Based Contrast Agents Engineered for Molecular Functional Magnetic Resonance Imaging

By

Vivian Hsieh

Submitted to the Department of Chemical Engineering
on May 20, 2016 in Partial Fulfillment of the
Requirements for the Degree of Doctor of Philosophy in
Chemical Engineering

## ABSTRACT

Magnetic resonance imaging (MRI) is a powerful neuroimaging tool that allows non-invasive visualization of the brain with high spatial and temporal resolution. Research on MRI contrast agents and their application to problems in neuroscience is burgeoning, and there is particular interest in developing MRI agents that are sensitive to time varying components of neurophysiology. Relatively recent advances in biomolecular probes has demonstrated the potential and versatility of bioengineered MRI sensors for molecular imaging. However, a major limitation of these probes is the high concentration needed for imaging, which can lead to issues such as analyte buffering and toxicity, and restrict the applicability of the sensors.

In this work, we explore two approaches for developing high relaxivity protein-based contrast agents to address the issues of low detectability. First, we coupled monoamine sensing with the disaggregation of superparamagnetic iron oxide nanoparticles (SPIOs). Ligand detection was imparted by integration of a monoamine sensing protein-based contrast agent derived from P450-BM3h (BM3). We demonstrated that this mechanism can produce robust signal changes of approximately 2-fold, while reducing the concentration of BM3 needed by 100-fold compared to the amount needed when only the protein is used for imaging. The second method demonstrated the feasibility of using semi-rational protein design to engineer a high relaxivity metalloprotein by tuning phenylalanine hydroxylase to bind gadolinium at high affinity. Mutations were found that increased the protein affinity by two orders of magnitude and enhanced relaxivity. The results of this thesis advance approaches for creating high relaxivity contrast agents which can be applied to the development of probes for other analytes, ultimately advancing and broadening the applicability of bioengineered probes in molecular functional neuroimaging.

Thesis Co-Supervisor: Alan P. Jasanoff
Title: Professor of Biological Engineering, Brain and Cognitive Sciences, Nuclear Science and Engineering

Thesis Co-Supervisor: K. Dane Wittrup
Title: Carbon P. Dubbs Professor of Chemical and Biological Engineering

## Acknowledgements

# Table of Contents

# 1 Introduction

Magnetic resonance imaging (MRI) was recognized soon after its invention as a potentially valuable tool for studying the central nervous system (CNS) and is now used extensively in the diagnosis of neurological disorders and in the study of cognition.[1,2] MRI is an attractive tool for examining neurobiology because of its relatively high spatial resolution (< 1 mm in humans, < 100 $\mu$m in animals) and ability to scan body tissues non-invasively. Contrast in MRI results from the distribution and dynamics of nuclear spins (usually arising from water protons) in a specimen, as well as the interaction of spins with applied radiofrequency and magnetic field gradient pulses. Contrast can be manipulated using molecular probes, which function as the MRI-equivalent of fluorescent dyes used in optical imaging. Although most MRI agents must be applied at high concentrations > $10^{-7}$ M (over a million times more than typical nuclear medicine probes) the versatility and precision of MRI and the fact that MRI probes can be sensitized to ligand binding or environmental factors present decisive advantages in contexts such as functional imaging. Research on MRI contrast agents and their application to problems in neuroscience is burgeoning, and there is particular interest in the possibility of finding MRI agents sensitive to time varying components of neurophysiology.[3]

The first generation of clinical contrast agents were salts and chemical complexes of paramagnetic metals, such as gadolinium (III) and manganese (II).[4-6] Complexes of these ions shorten the longitudinal ($T_1$) and transverse ($T_2$) relaxation times of nearby water molecules, properties that determine, respectively, the rate with which an MRI signal can be repeatedly measured and how long the signal persists during an individual measurement period. Increases in $T_1$ relaxation due to a contrast agent produce image brightening in MRI, whereas increases in $T_2$ relaxation produce image darkening. In either case, contrast is enhanced where the relaxation-

based contrast agent localizes. Molecular probes can produce MRI contrast based on alternative mechanisms as well. So-called chemical exchange saturation transfer (CEST) agents work by providing a probe-specific nuclear magnetic resonance frequency via which radiofrequency irradiation can be applied to diminish the local MRI signal.[7] Heteronuclear probes allow MRI to be performed using nuclei other than protons, such as $^{19}F$ and $^{129}Xe$, which are not normally found in living subjects.

Most MRI contrast agents are low molecular weight metal complexes prepared by synthetic chemistry, but notable recent advances have followed from the development of bioengineered macromolecular and supramolecular MRI probes. The biophysical properties that allow some proteins to act as contrast agents were established even before MRI came into use as a clinical imaging tool.[8,9] It has also long been known that synthetic relaxation agents experience increases in potency ($T_1$ or $T_2$ relaxivity, denoted $r_1$ or $r_2$ and equal to the slope of relaxation rate $vs.$ concentration) upon binding proteins; this follows from the dependence of relaxivity on molecular rotational correlation time. The use of biomolecules and biomolecule conjugates as contrast agents $themselves$ confers additional key advantages, however. The amenability of biomolecules to molecular engineering allows for the facile development of probes with novel functionality such as target binding or ligand responsiveness. With some biomolecular contrast agents, there is the additional possibility of genetically encoding them, for $in$ $vivo$ application as gene reporters or to enable endogenous synthesis in targeted cells. Several of these advantages extend to "hybrid" bioengineered contrast systems, in which biomolecules are designed to interact with synthetic components to produce MRI contrast patterns of physiological interest.[10] The subsequent sections of this chapter explore the unique properties of bioengineered MRI

probes in greater detail, highlighting opportunities to apply the new bioengineered molecular MRI techniques in neurobiological systems.

## 1.1 Amenability of biomolecular contrast agents to engineering

The discovery of green fluorescent protein (GFP)[11] and its homologues in marine organisms led to a dramatic synthesis of genetic and imaging techniques based on light microscopy.[12] Molecular engineering techniques have since been applied to construct fluorescent protein-based sensors, to assemble reporters incorporating fluorescent proteins, and to tune the fluorescence properties of GFPs. Nature has been comparatively generous in providing MRI-detectable proteins—candidate "GFPs for MRI." There are numerous paramagnetic proteins, for instance, which are capable of producing $T_1$ or $T_2$ contrast in MRI. These proteins can be targets for bioengineering techniques in much the way that GFP has been. Molecular engineering can also be applied to design and tune diamagnetic probes or components of hybrid agents.

The most important MRI-detectable protein in neuroscience research is hemoglobin, which is a paramagnetic in its unliganded form but diamagnetic when oxygen bound;[13] the effect of neurovascular coupling responses on the equilibrium between these two forms underlies the blood oxygen level-dependent effect used for functional MRI (fMRI).[14-16] Hemoglobin might seem like a promising starting point for the development of analyte-sensitive MRI molecular imaging probes, and in fact a chemically-modified form of the molecule has been applied as an exogenous $T_2$ contrast agent for tissue oxygen tension imaging *in vivo*.[17]

Of various heme-containing molecules, hemoglobin is not the most amenable to further bioengineering however, in part because of its heterotetrameric structure, and also because its

binding pocket is too shallow for specific interactions with potential ligands. By applying

molecular engineering techniques to another heme protein, a bacterial cytochrome P450 domain

(BM3h), Shapiro et al. produced a contrast agent sensitive to the neurotransmitter dopamine

(Figure 1a).[18] The authors found that binding of a natural ligand, arachadonic acid, alters the $T_1$

relaxivity of BM3h by displacing a water molecule coordinated to the heme iron. They then

applied a technique called directed evolution,[19] which involves random mutagenesis followed by

screening over repeated rounds of optimization, to tune the BM3h binding specificity away from

arachidonic acid and towards dopamine. The resulting sensors had dopamine binding affinities of

3.3-8.9 $\mu$M and were shown to detect extracellular dopamine in both cell culture and rat brains.

Further work was done to enhance the relaxivities of BM3h mutants by substituting the native

heme with a high spin manganese (III) protoporphyrin complex.[20] Both directed evolution and

metal substitution can be generally applicable approaches for bioengineering of MRI contrast

agents. Directed evolution in particular is a powerful technique because it does not require *a*

*priori* knowledge of how mutations affect protein structure and function; the technique can

therefore be applied to alter the properties of almost any naturally occurring or artificially

constructed biomolecular probe.

Rational protein design methods are complementary to screen-based techniques like

directed evolution, and have also proved useful in the development of MRI probes. Several

groups have constructed contrast agents by conjugating modified proteins to superparamagnetic

iron oxide (SPIO) nanoparticles. In one study, Atanasijevic et al. developed a MRI sensor for $T_2$-

weighted imaging of calcium ions,[21] which are well known as ubiquitous intracellular signalling

molecules in the nervous system. The sensor consisted of one set of SPIOs conjugated to the

calcium-binding protein calmodulin (CaM) and another conjugated to a target peptide that

interacts with CaM only in its calcium bound form. Mixtures of the SPIO populations aggregated in the presence of increased calcium concentrations, producing approximately 5-fold changes in $T_2$-weighted MRI signal *in vitro* by a mechanism very distinct from earlier synthetic calcium sensors.[22,23] Using wild-type CaM, the sensor had a transition midpoint of approximately 1 $\mu$M $Ca^{2+}$, but when rationally designed point mutations were introduced into the interacting protein domains, both the midpoint and cooperativity of the sensor's calcium-dependent response could be tuned (Figure 1b).[21,24] The process of adjusting the properties of a reagent using site-directed mutagenesis is much simpler than the resynthesis that would be required with a more conventional chemical contrast agent, and again illustrates the advantage of bioengineering techniques in MRI probe development.

Using biological engineering, MRI probes can also be created from scratch. *De novo* design was used recently to create diamagnetic metal-free proteins capable of being visualized by the CEST contrast mechanism in living rodent brains.[25] Any molecule that contains a labile proton pool in exchange with bulk water can function as a CEST agent, provided that the exchange takes place on an appropriate time scale and that the chemical shift of the bound protons is sufficiently resolved from bulk water. Several amino acid sidechains, such as those of lysine, arginine, and tryptophan, contain protons that effectively support CEST contrast, and can be incorporated into polypeptides to construct genetically encoded CEST reporters. In the first demonstration of this principle, Gilad *et al.* designed a lysine rich protein that displayed specific contrast in cells expressing the construct[25]. Implanted tumors expressing LRPs could be detected by CEST-weighted MRI in rat brains and distinguished from unlabeled tumours. The same group also demonstrated that the magnitude and frequency of protein-associated CEST effects could be tuned by altering the amino acid sequence (Figure 1c).[26] McMahon *et al.* screened an array of

peptides composed of combinations of lysine, arginine, and threonine to obtain CEST agents that could be detected differentially. This raises the possibility of performing a form of "multicolor" imaging using several distinct CEST reporters in parallel, and exploits both the combinatorial nature and easy synthesis of biopolymers.

## 1.1  Imaging with biomolecular catalysts

Efforts to create biosynthetic MRI contrast agents are benefiting not only from the powerful molecular engineering approaches that can be used, but also from the unique capabilities of biomacromolecules as imaging agents or components of molecular imaging strategies. Perhaps the most famous example of this is the ability of proteins to act as highly specific catalysts. Enzymes have been used for decades in optical imaging, originally as markers visualized by histology and more recently in combination with bioluminescent and fluorescent substrates for *in vivo* imaging.[27] Now a host of enyzmes have been explored for their ability to induce contrast in molecular MRI experiments, in conjunction with various mechanisms for coupling MRI contrast to chemical processing (Figure 2). Although some of the enzymes used in these studies are disease-related markers, as opposed to established gene reporters, the strategies used to detect these molecules (and in some cases the enzymes themselves) could be adapted for use in reporter systems or alternative MRI detection specificities as well.

One of the earliest demonstrations of reporter enzyme detection using MRI was the mapping of the $\beta$-galactosidase ($\beta$-gal) activity in whole frog embryos with a $\beta$-gal-sensitive $T_1$ contrast agent (Figure 2a).[28] In this work, Louie *et al.* created a $Gd^{3+}$ macrocyclic attached to a galactose group, joined by a linker that is cleavable by $\beta$-gal. Enzymatic hydrolysis of the

contrast agent exposes the paramagnetic ion to water molecules, resulting in an increase in $T_1$ relaxivity. Because the contrast agent was injected intracellularly at an early stage in embryogenesis, numerous structures, including the head, could be visualized in the presence of β-gal activity in these experiments. Although β-gal is perhaps the most widely used reporter enzyme in biological research, the difficulty of delivering the contrast agent has impeded efforts to apply the technique for gene expression mapping in additional contexts.

In another example, a lipid-modified $Gd^{3+}$ chelate-based contrast agent was developed by Himmelreich *et al.* and used to detect intracellular lipase activity in cells.[29] Prior to enzyme processing, the contrast agent was insoluble and did not alter MRI signal. However, once internalized via phagocytosis by cells expressing lipases, the fatty acid chains were cleaved from the compound, solubilizing the $Gd^{3+}$ chelate to produce strong $T_1$ contrast. A very different contrast mechanism also involving hydrolysis of a gadolinium compound was used to monitor activity of the protease caspase-3 in a recent study. Mizukami *et al.* created a probe consisting of gadolinium-tetraazacyclododecanetetraacetic acid (Gd-DOTA) conjugated to the peptide sequence DEVD and an ^{19}F-containing group potentially detectable by heteronuclear MRI (Figure 2b).[30] The short peptide brings the $Gd^{3+}$ in close proximity to the fluorine atom, promoting relaxation of the ^{19}F signal on a timescale too short for measurement by MRI. The action of the enzyme cleaves off the fluorinated moiety and removes the intramolecular relaxation effect, allowing the ^{19}F MRI signal to be detected. Although ^{19}F MRI is a relatively insensitive technique in general, the enzyme can provide amplification by processing many copies of the substrate; *in vitro* at least the caspase-3 reaction could be effectively monitored.

Qualitatively different enzyme-catalyzed chemical reactions, involving neither cleavage nor hydrolysis, can also potentially become the basis for MRI detection schemes. Rodriguez *et*

*al.* synthesized $Gd^{3+}$ chelates that could be oxidized by myeloperoxidase (MPO),[31] an enzymatic marker associated with inflammation. Oxidized contrast agents tended to oligomerize and crosslink via phenolic side groups of tyrosine residues, increasing $r_1$ by up to 1.5 fold, due to the dependence of relaxivity on the timescale for molecular motion (Figure 2c). MPO activity has also been coupled to the aggregation of serotonin-functionalized SPIOs.[32] The phenolic group acts as the electron donor group and is converted to a tyrosyl radical when MPO reduces hydrogen peroxide. Formation of tyrosyl radicals by peroxidases induced cross-linking and aggregation of the nanoparticles, creating $T_2$ changes. A somewhat related strategy could be used to detect the enzyme tyrosinase, which catalyzes serial oxidation steps that lead to the formation of melanin polymers, which in turn promotes paramagnetic metal ion accumulation in cells and consequent MRI changes.[33] The activity of overexpressed tyrosinase recapitulates the process whereby neuromelanin forms in cells of the substantia nigra in the brain, a region known for high iron content and $T_2$ MRI contrast.[34]

Enzymatic detection schemes for MRI have been developed around nanoparticle contrast agents as well as small molecules. Nanoparticle $T_1$ and $T_2$ contrast agents are particularly advantageous because of their high relaxivities.[35] In one of the first examples of this, *in vivo* expression of an engineered transferrin (Tf) receptor in mice was detected using Tf-conjugated SPIOs.[36] The Tf-SPIOs are transported into the cell by receptor-mediated endocytosis, allowing tumor cells to be imaged and tracked. A similar accumulation-based mechanism has also been demonstrated with SPIOs coated with a "masked" version of a cell penetrating peptide (CPP).[37] Matrix metalloproteins (MMPs) are proteases with activities highly linked to tumor invasion and metastasis.[38] Olsen *et al.* used an MMP substrate peptide consisting of a polyarginine CPP sequence separated by the MMP cleavage site from a polyglutamate stretch expected to block

CPP function;[37,39] peptides were conjugated to fluorescent and Gd-DOTA-labeled dendrimers (Figure 2d). The action of MPP-2 or MMP-9 cut off the polyglutamate masking region, allowing the peptides to be taken up by cells due to the unmasked CPP function. The authors observed accumulation of the probe at the invasive edges of MMP-expressing tumors by fluorescence, as well as $T_1$ relaxation changes of up to approximately 30%. The use of dendrimers reduced the clearance rate of Gd-DOTA and apparently limited its non-specific uptake by tissues, thus improving the contrast between MMP-expressing structures and other tissue.

Another nanoparticle-based enzyme detection scheme was developed by Westmeyer *et al.*, who applied an MRI sensor to detect enzymatic turnover catalyzed by secreted alkaline phosphatase (SEAP),[40] a reporter used previously to visualize gene expression patterns in the brain. Bioengineering of an MRI technique around a secreted enzyme obviates the need for intracellular delivery, in contrast to strategies for β-gal detection.[28,41–44] Further, the use of a contrast agent to detect products of the enzyme, as opposed to functioning as substrates themselves, facilitates dynamic studies of enzyme activity, since the contrast agent is not irreversibly modified over time. An unnatural nucleotide 2'-adenosine monophosphate is processed by SEAP into adenosine (Ado), which is then detected by an Ado sensor for MRI (Figure 2e). Ado acts on the sensor by inducing disaggregation of SPIO nanoparticles crosslinked by a switchable DNA aptamer;[45] the aggregation state influences changes in $T_2$ relaxivity which can be detected by MRI. A nanoparticle $T_2$ contrast agent based on the enzymatic degradation of a polymer coating has also been explored as a possible gene reporter component.[46] In this strategy, commercial SPIOs coated with a relatively thick coat of dextran (Feridex) were substrates for the enzyme dextranase. Enzymatic digestion of the nanoparticle coating exposed the iron oxide core to water, producing $T_2$ changes both *in vitro* and *in vivo*.

## 1.2 Bioengineering of targeted imaging agents

The promise of applying contrast agents for diagnosis of disease, both inside and outside the brain, drives a major portion of molecular imaging research. The disadvantageous sensitivity of MRI compared with positron emission tomography is compensated in many cases by MRI's superior resolution, and low sensitivity is not necessarily a barrier in cases where substantial amount of imaging agent can be delivered to sites of action, e.g. in the bloodstream. Many targeted MRI probes developed to date include biological components, in large part because of the high specificity imparted by macromolecular ligands. To produce targeted contrast agents, biomolecular domains can be chemically conjugated to passive synthetic contrast agents such as paramagnetic metal complexes, SPIOs, and dendrimers (Figure 3). An early example was offered by Sipkins et al., who used monoclonal antibodies labelled with paramagnetic liposomes to target the angiogenesis marker integrin $\alpha_v\beta_3$.[47] The anti-integrin antibody was conjugated to the liposomes through biotin-avidin conjugation. They demonstrated that the integrin-targeted liposome could be used to image angiogenic vasculature and distinguish between benign and malignant tumor phenotypes in rabbits, a distinction that could not be made with conventional MR imaging techniques. An integrin binding partner, VCAM-1, has also been targeted in a more recent approach that enabled detection of acute endothelial inflammation in mouse ears[48] and brains.[49] Here a monoclonal antibody against VCAM-1 was conjugated to SPIO microparticles, which are individually detectable by MRI. In another study, an intravascular agent designed for detection of fibrotic lesions was prepared by conjugating a gadolinium chelate to a collagen binding peptide identified by phage display.[50-53] The use of phage display or related affinity-

based polypeptide screening methods to produce targeting motifs for molecular imaging agents represents a prime example of how biological engineering techniques can advance this field.

Targeted MRI probes of potential utility in basic neuroscience have been formed by conjugating contrast agents to proteins that are spontaneously taken up and transported along neural fibers. Early attempts at this was based on conjugation of wheat germ agglutinin (WGA), a predominantly anterograde tracer, to SPIOs.[54-56] Using WGA-SPIO conjugates, bidirectional slow axonal transport could be visualized as migrating hypointensity in rodent peripheral nerves, but analogous transport could not be seen in the CNS. However, Wu et al. achieved successful tract tracing results in the brain using a gadolinium-DOTA conjugate of the cholera toxin B subunit (CTB),[57] an established retrograde tract tracer.[58] Injections of the MRI tracer into somatosensory cortex of rats produced hyperintense $T_1$-weighted MRI signal in projections arising from thalamic nuclei, and injections into olfactory bulb labelled olfactory regions of the cortex.[57] The comparative success of the Gd-based tracer compared with WGA-SPIO conjugates for tract tracing in the CNS suggests the potential for modifications of larger size to interfere with properties of proteins they are conjugated to.

Biological macromolecules other than proteins have also been used to engineer targeted imaging agents for in vivo MRI. In one study, so-called glyconanoparticles consisting of iron oxides modified with carbohydrates were created to bind the endothelial marker proteins E and P-selectin.[59] Like VCAM-1 and integrin-targeted conjugates, these imaging agents were also able to detect vascular hallmarks of cerebral inflammation in rodent brains. Oligonucleotide aptamers attached to MRI contrast agents also permit targeting to protein epitopes. In one study, an aptamer-conjugated SPIO contrast agent was used to detect the coagulation factor thrombin in vitro; detection of concentrations as low as 25 nM was reported.[45] The possibility of producing

aptamers against a wide variety of targets using systematic evolution of ligands by exponential enrichment (SELEX) technology[60,61] may lead to further examples of nucleic acid-based molecular MRI agents. Even more exciting is the possibility of targeting oligonucleotide conjugates to DNA and RNA molecules themselves, especially in the CNS. In a series of papers, Liu and coworkers have described MRI experiments in which oligonucleotide conjugated SPIOs were applied to detect specific gene transcripts in rodent brains, in an MRI-based version of *in situ* hybridization mapping.[62-64] The authors found contrast patterns dependent on the oligonucleotide targeting sequences they used, and on stimuli delivered in conjunction with the MRI probes. This approach requires that the contrast agents permeate the blood brain barrier (BBB), as well as individual cell membranes, and evidence of both was reported.[65]

The difficulty of delivering contrast agents past the BBB poses a unique challenge for targeted molecular imaging of most ligands in the brain.[66] A particularly interesting solution to this problem is the possibility of producing the contrast agents directly within the brain, using DNA constructs which may be targeted using genetic techniques. Although genetic approaches are not yet on the horizon for clinical molecular MRI, basic scientific applications may benefit considerably from the fusion of imaging with genetic technologies.[10,67] The metalloprotein ferritin (Ft) stores endogenous iron as a crystalline ferrihydrite core which has been shown to influence MRI contrast where it is naturally expressed. Genove *et al.* showed that viral-mediated overexpression of Ft in the mouse brain produces clear $T_2$ signal changes by enhancing iron loading in the transduced neurons,[68] and Cohen *et al.* showed altered $T_2$ contrast patterns in transgenic mice expressing Ft as a marker for endothelial cells in the brain and elsewhere.[69,70] Although Ft is similar in size and iron content to synthetic SPIOs, its relaxivity is over 100 times lower due to the relatively amorphous and hydrated mineral structure of its core.[71] Strategies

have been explored to improve Ft relaxivity, such as co-expressing transferrin receptor to transport more iron into cells.[72] Through a directed evolution approach that screens for reduced cytosolic iron concentration, Matsumoto et al.[73] isolated a mutant of Ft from *Pyrococcus furiosus* (SPFt) which sequestered almost twice the amount of iron and showed approximately 2-fold increase in relaxivity compared to the wild type protein. Additional genetically encodable MRI reporters have also been explored, including ion transporters such as MagA,[74,75] a protein from magnetotactic bacteria. Several groups have also demonstrated changes in MRI due to expression of diamagnetic proteins, including the lysine-rich CEST reporters described above,[25,26,76,77] and GFP, which was detected by magnetization transfer-weighted imaging.[78] An advantage of genetically encoded diamagnetic agents is that their expression and resultant contrast do not require association with or accumulation of a paramagnetic cofactor.

## 1.3 Limitations of bioengineered MRI probes

Advances have been made in the design of new MRI contrast agents that could eventually further our understanding of the brain and its diseases. Most MRI probes, however, have not progressed past the proof-of-principle stage. Many are limited by their low sensitivities,[66] as demonstrated by the high probe concentrations applied in published studies. Although low sensitivity is a problem for all MRI contrast agents, it is more of a challenge for existing biomolecular contrast agents than for synthetic agents. The problem is exemplified by protein $T_1$ agents like BM3h, which has a relaxivity of 1.23 $mM^{-1}s^{-1}$ at 21 °C and 4.7 T,[18] compared with 3-5 $mM^{-1}s^{-1}$ for $Gd^{3+}$ compounds under similar conditions.[4] The relaxivity of Ft is also much lower than that of synthetic SPIO contrast agents, ~1 $(mM\ Fe)^{-1}s^{-1}$ for Ft[79] vs. 50-200 $(mM\ Fe)^{-1}s^{-1}$ for typical

SPIOs.[80] Protein-based CEST agents also offer relatively low sensitivity, compared with synthetic CEST agents that incorporate chelated lanthanides.[81] With today's technology, a synthetic MRI contrast agent is therefore likely to be applicable at lower concentration and with lesser risk of physiological disruption or toxicity than a biomolecular probe. This is one reason why much effort has focused on detection systems in which small molecule synthetic contrast agents function as responsive substrates for enzymes that provide amplification as well as desirable targeting and specificity properties.

For neuroimaging applications, a second confounding issue is the difficulty of delivering contrast agents noninvasively to the brain.[82] Because almost all MRI contrast agents are polar, charged compounds, BBB permeability is not spontaneously achieved. For applications in humans, the problem of trans-BBB delivery has almost entirely prevented CNS applications of MRI contrast agents, except for imaging cerebrovascular parameters. In animals, BBB disruption using hyperosmotic shock or ultrasound has been used to deliver agents ranging from small molecules[83–85] to nanoparticles[86–88] into the brain parenchyma. Although they are not yet common techniques in the clinic, both osmotic shock[89] and focused ultrasound-mediated[90] BBB disruption techniques have also been applied in human or nonhuman primate subjects. Even using these methods, however, larger molecules are difficult to deliver. A systematic study of ultrasound-mediated delivery of fluorescent dextrans of varying size found for instance that a 3 kD molecule (comparable to a short peptide) could be delivered at approximately five-fold higher doses than a 70 kD molecule (comparable to a medium-sized protein).[91] Molecules in the megadalton size range were not effectively delivered. For bioengineered protein probes or nanoparticle bioconjugates, compared with "conventional" small molecule MRI contrast agents, the BBB delivery problem clearly poses a particular challenge therefore. One way to bypass the need for

trans-BBB delivery is to use genetic targeting to the brain, in conjunction with protein-based agents. Although this is an exciting approach to use in transgenic animals, it cannot yet be contemplated in humans. Moreover, because of the relatively low sensitivity afforded by existing genetically encoded contrast agents, achieving high enough expression levels to produce desired MRI contrast levels in cells or tissue is not easy.

Both the sensitivity and delivery limitations of bioengineered MRI probes may reflect the current "state of play," as opposed to theoretical constraints, however. Biomolecular relaxation agents for instance, can in principle reach relaxivity levels considerably higher than current synthetic contrast agents.[92-95] High $T_1$ relaxivity depends on interplay between electronic relaxation and solvent interaction parameters that might indeed be easier to optimize in macromolecular agents than with synthetic probes, due to the amenability of biomolecules to tuning and screening approaches. Large magnetic moments characteristic of synthetic SPIOs might also be achieved in biological systems, and have naturally occurring precedents in the magnetosomes of magnetotactic bacteria,[96] as well as mineral deposits found in several vertebrate species.[97-100] Improving the sensitivity of biomolecular MRI contrast agents will also enable them to be used at concentrations where immunogenicity, an intrinsic property of these types of probes, will be less significant. Meanwhile, brain delivery of macromolecules could be enhanced by fusion to so-called Trojan horse vehicles, like transferrin, which are themselves proteins and have been shown to deliver cargo to the brain.[101] In conjunction with improved genetically encoded contrast agents, trans-BBB viral delivery strategies may also one day prove effective for noninvasive brain delivery biosynthetic MRI probes. Some types of virus have been shown to cross the BBB spontaneously[102-104] and could serve as vectors for this purpose, at least in animals. In fact, variants of adeno-associated viruses (AAVs) have been developed from a

novel Cre recombination-dependent screening approach that enable global CNS transduction of adult mice.[105]

## 1.4 Conclusions

In the wake of the genetic and genomic revolutions, the expansion of biology-based technologies into multiple spheres of investigation has been dramatic. Protein therapeutics are becoming widespread, and some are being actively investigated for CNS applications. In the area of molecular neuroimaging, which seeks to monitor neural structure and function at a molecular level for both research and clinical purposes, bioengineering methods are having impact largely via the development of new probes. New concepts for design of molecular MRI agents have emerged from the use of biomolecules as templates or building blocks. Strategies for discovering and enhancing contrast agents have been borrowed from the palette of macromolecular engineering techniques available to researchers across the life sciences. Although there are substantial limitations to the currently available molecular MRI methods, the bioengineering approaches recently demonstrated in this field provide a strong foundation for continued innovation of MRI-based measurement modalities that could over time change the way brains are studied and diagnosed. In my thesis, I investigate approaches for addressing the sensitivity limitations bioengineered contrast agents. The first strategy looks to improve the sensitivity of an existing set of monoamine neurotransmitters by coupling detection with the robust MRI signals of superparamagnetic iron oxide nanoparticles (Chapter 2). The second method investigates the feasibility of using semi-rational protein design towards developing high relaxivity metalloprotein-based sensors (Chapter 3).

# Figure 1. Bioengineered MRI probes



**a** DNA library construction · protein expression · high throughput screening · analysis of top candidates · mutations shift ligand specificity

**b** protein actuating domains · wild-type · mutant · sensor response · log([Ca²⁺])

**c** S/S₀ · ppm

# Figure 2. Strategies for MRI-based detection of enzyme activity

**a**

β-galactosidase

increased relaxivity

hydrolysis

**b**

caspase-3

hydrolysis

fluorine MRI signal amplified following cleavage

**c**

myeloperoxidase

oxidation

dimerizes, reacts with proteins, altering relaxivity

**d**

matrix metallo-protease-2

cleavage "unmasks" CPP, promotes contrast agent uptake

hydrolysis

PLGC(Me)AG-rrrrrrrrr-c
└──(PEG2)-eeeeeeee-Suc

**e**

secreted alkaline phosphatase

dephos-phorylation

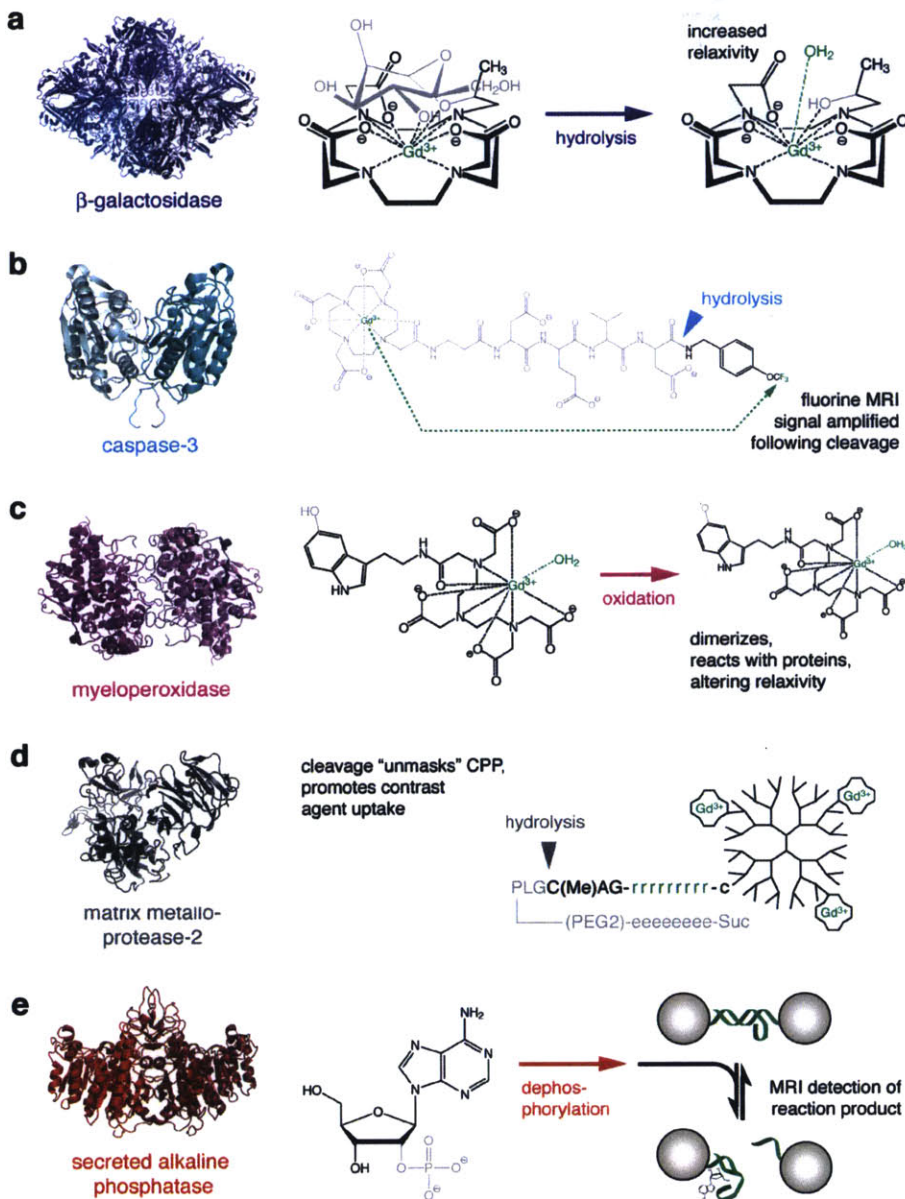MRI detection of reaction product

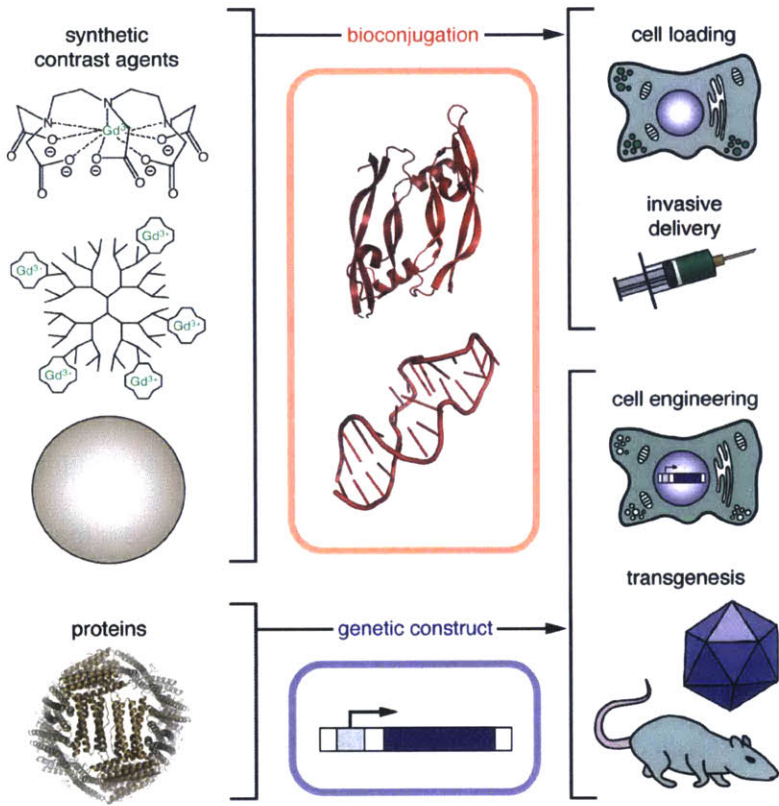# Figure 3. Biomolecule-based targeting of MRI contrast agents

**Figure Legends**

**Figure 1. Bioengineered MRI probes. (a)** Directed evolution strategy was used by Shapiro *et al.* to produce dopamine-sensitive MRI contrast agents from the heme domain of the cytochrome P450 BM3 heme domain (BM3h). The wild-type BM3h gene is randomly mutated to produce a DNA library. The library is transfected into E. coli and variant proteins are expressed in multiwell format. Cells are lysed and lysates screened by titration with dopamine and the wild-type ligand arachidonic acid. Variants showing the greatest enhancement in dopamine binding and decrement in arichidonate binding are analyzed in purified form to assess ligand responsiveness and relaxivity changes. The process is repeated over multiple cycles to produce progressive improvement in target ligand responsiveness. The right-hand panel shows the distribution of mutations (blue spheres) selected by directed evolution of BM3h (gray Cα trace), depicted in complex with its heme group (orange) and wild type arachidonate ligand (black).[18] **(b)** Rational protein design can be applied to tune properties of a biomolecule-actuated MRI sensor. Calcium-dependent protein-protein interactions drive responsiveness of a superparamagnetic iron-oxide (SPIO) based sensor developed by Atanasijevic *et al.* Calmodulin (red) and its peptidic binding partner (cyan) are conjugated to two populations of SPIO nanoparticles (left); reversible clustering takes place in the presence of calcium and leads to $T_2$ changes. By mutating the protein domains (inset), the midpoint and cooperativity of the sensor's response can be altered (schematic graph, right).[21] **(c)** *De novo* bioengineering produces protein-based chemical exchange saturation transfer (CEST) contrast agents. Probe-specific CEST contrast is produced by an MRI pulse sequence (top left) in which a radiofrequency saturation pulse (red) is delivered at the frequency of an exchangable proton pool associated with the CEST

reporter (blue arrowhead); because of chemical exchange, the saturation is transferred to protons at the frequency of bulk water (cyan). MRI signal decreases are observed as a function of frequency, as reflected in the so-called Z-spectrum (graph at bottom left). McMahon *et al.* showed that peptides can be designed to contain labile proton pools associated with a variety of specific chemical shifts (color coding in structures at right). Each proton pool produces a corresponding signature in the Z-spectra at left (color-coded arrowheads), allowing the molecules to be distinguished by CEST-weighted MRI.[26]

**Figure 2. Strategies for MRI-based detection of enzyme activity.** For each example, the structure of the enzyme is shown at left, and the reaction catalyzed is shown at right. The chemical moieties most directly affected by the enzyme are shown in gray, and molecular components most directly responsible for MRI contrast are shown in green. **(a)** Gadolinium-containing substrate for β-galactosidase. Enzyme activity cleaves off a sugar moiety, increasing exposure of the gadolinium atom to interaction with a water molecule and consequently increasing $T_1$ relaxivity.[28] **(b)** Peptide-based probe for ^{19}F MRI-based detection of caspase-3 activity. Prior to cleavage, the relaxation enhancement caused by the gadolinium chelate at left prevents detection of an ^{19}F signal arising from the trifluoromethyl group at the right. Action of the enzyme cleaves removes the gadolinium-containing fragment and relieves the intramolecular relaxation effect, allowing an ^{19}F signal to be detected.[30] **(c)** Myeloperoxidase oxidizes the 5-hydroxy group of a serotonin-conjugated gadolinium chelate. The resulting free radical species tends to dimerize and react with proteins, resulting in compounds with longer $\tau_R$ and higher relaxivity.[31] **(d)** A gadolinium-bearing dendrimer is conjugated to a peptide containing a poly-D-arginine cell penetrating domain, "masked" by an oppositely charged poly-D-glutamate domain.

Action of matrix metalloprotease-2 or -9 cleaves the peptide, unmasking the polyarginine fragment and promoting accumulation of the contrast agent in nearby cells.[37] **(e)** Detection of the reporter enzyme secreted alkaline phosphatase (SEAP) is performed using a nanoparticle-based $T_2$ MRI sensor that detects adenosine, a product of SEAP-mediated dephosphorylation of 2'-adenosine monophosphate (left). Removal of adenosine by transport or further enzymatic processes reverses the contrast change mediated by the sensor.[40]

**Figure 3. Biomolecule-based targeting of MRI contrast agents.** Bioengineering approaches are used to target both synthetic and genetically encoded MRI contrast agents to the nervous system or elsewhere. Synthetic contrast agents (top) may be conjugated to macromolecular domains (proteins, nucleic acids, or oligosaccharides) for targeted delivery. The resulting semi-synthetic agents are introduced into experimental subjects either by loading and introducing cells (*e.g.* for cell tracking or monitoring), or by direct injection into the bloodstream or brain. Protein-based agents (bottom) can be targeted for endogenous production using genetic constructs. DNA vectors are used to engineer cells to express the contrast agent, or to induce contrast agent expression directly in animals via viral-mediated gene transduction or transgenesis. Neurotransmitter detection coupled with disaggregation of iron oxide nanoparticles

## 2    Design of T2 relaxivity MRI sensor for high sensitivity detection of monoamine neurotransmitters

### 2.1    Introduction

Magnetic resonance imaging (MRI) is a non-invasive imaging technique with relatively high spatial and temporal resolution, making it a powerful tool for studying neural activity. The predominant approach for functional neuroimaging (fMRI) has been blood-oxygen-level-dependent (BOLD) fMRI, which is based on the oxygenation of hemoglobin in blood.[14] Based on cerebral hemodynamics, BOLD fMRI lacks specificity and temporal precision due to the complexity of neurovascular coupling, resulting in slow and indirect readouts of neural activity.[106] Contrast agents have long been used to enhance MRI signal and there have been recent advances which impart contrast agents with functionality, target binding, or ligand responsiveness using biomolecules or biomolecular conjugates.[107] The specificity of probes such as these could be used to obtain direct measurements of brain activity with higher precision and faster response kinetics compared to BOLD fMRI.[3]

Previously, monoamine-sensitive protein-based contrast agents were developed through directed evolution of the heme domain of bacterial cyctochrome P450-BM3 (BM3h).[18,108] The dopamine-responsive mutant, BM3h-9D7 (9D7), was evolved as a $T1$-based imaging agent[108] and has been applied to *in vivo* imaging of dopaminergic signaling.[109] Lee *et al.* demonstrated that the protein could be used for functional MRI (fMRI) of reward-based behavior in rats. A mutant that detects serotonin, BM3h-2G9C6 (2G9C6), was also developed[108] and was used in a fMRI study of serotonin reuptake pathways in live rats.[110] The study demonstrated that the

sensor could be used to map serotonin transport pathways and investigate pharmacological effects on neural pathways. However, the limitation of these sensors and other existing biomolecular probes is the high concentrations ($> 10^{-6}$ M) that must be applied compared to synthetic agents. In the BM3h *in vivo* studies, 20 μM of sensor was required in order to detect physiological levels of neurotransmitters.[109,110] 2G9C6 also had to be injected as a preformed complex with serotonin at high micromolar concentrations in order to be detected. Furthermore, amperometric recordings in the dopamine study confirmed that the high sensor concentration buffered a significant portion of the neurotransmitter released during signaling. The conditions required for these studies indicate that the sensitivities of the BM3h sensors need to be improved in order to broaden the utility of these sensors in molecular fMRI.

To do so, the BM3h proteins were incorporated with high relaxivity superparamagnetic iron oxide nanoparticles (SPIOs) to create a class of *T2*-weighted contrast agents for the detection of monoamine neurotransmitters. The proteins will serve as the ligand binding domain, with the MRI signal derived from the SPIOs. SPIO-based contrast agents have been shown to be detectable at nanomolar concentrations and total iron concentrations an order of magnitude lower than conventional imaging agents. This integration of BM3h ligand affinity with the robust signal of SPIOs will allow for imaging of monoamine signaling with lower concentration of imaging agent, reducing the risk of physiological disruption and toxicity.

## 2.2 Results and discussion

**Sensor design**

Analyte-specific MRI sensors have been developed using SPIOs by coupling the presence or activity of the analyte with a nanoparticle aggregation state. In each case, crosslinks between the nanoparticles are either formed or disrupted by the analyte of interest.[107,111] The change in the spatial distribution of nanoparticles subsequently induces dramatic changes in $T2$ relaxation, which can be detected by MRI.[112] In this work, dopamine or serotonin release is sensed by detecting the dispersion of SPIO clusters. The sensor is comprised of two distinct SPIO populations: one set functionalized with a BM3h variant, and another set coated with a neurotransmitter analog. In the absence of free neurotransmitter, mixtures of these nanoparticle species form aggregates through protein-ligand binding interactions between the immobilized protein and neurotransmitter analogs. Neurotransmitter in solution competes for the ligand binding sites of the protein and disrupts the interaction between the nanoparticles, which causes the nanoparticle clusters to disaggregate and produce contrast changes (Scheme 1).

The nanoparticles used in this study were maleimide-terminated photocrosslinked lipid iron oxide (pcLCIO) nanoparticles with 10 nm diameter SPIO cores. This method of SPIO functionalization has previously been shown to produce more compact sized superparamagnetic particles with enhanced stability in solution.[113] The pcLCIOs were conjugated to BM3h *via* native cysteine residues and a site-specific cysteine residue introduced near the C-terminus of the protein. BM3h has three native cysteine residues: C400 which coordinates with the heme iron, and C62 and C156 which are on separate alpha helices and do not interact. Without introducing additional cysteine residues, protein quantification showed that BM3h can be conjugated to

pcLCIO *via* thiol-maleimide chemistry at levels of 36 ± 1.6 mol BM3h per mol of pcLCIO. The mutation S450C allowed pcLCIOs to be modified with up to 71 ± 15 mol BM3h per mole of pcLCIO, likely because the mutation incorporated a more accessible cysteine residue. Increased degree of modification is desired because aggregation kinetics have been shown to be accelerated by higher density of surface functionalization moieties.[113] The dopamine and serotonin *T2* agents used pcLCIOs conjugated with 9D7 and 2G9C6, respectively. The S450C mutation was introduced into both BM3h variants without greatly affecting ligand binding affinities. 9D7 binds dopamine with $K_d$ of 1.3 ± 0.1 $\mu M$[108] without the mutation, and $K_d$ of 2.6 ± 1.4 $\mu M$ with the mutation. 2G9C6 binds serotonin with $K_d$ of 0.7 ± 0.1 $\mu M$[108] and 1.6 ± 0.6 $\mu M$ without and with the S450C mutation, respectively. After protein conjugation, the diameter of the BM3h-pcLCIOs was found to be 38 ± 5 nm by dynamic light scattering (DLS).

**PEGylated ligand synthesis**

We needed to synthesize novel tethered monoamines for conjugation to pcLCIOs due to the binding orientation of neurotransmitters in BM3h. From crystal structures, neurotransmitters are known to bind via corrdination of the primary amine with heme group iron,[108] rendering the amine groups unavailable for conjugation chemistry. Given the chemical structures and the binding orientations, the monoamines had to be modified at the hydroxyl positions. Additionally, the molecules had to contain a thiol group to facilitate thiol-maleimide chemistry with the pcLCIOs and a spacer to extend out of the ligand binding pocket and prevent steric effects from a thioether bond that could reduce binding affinity between the tethered ligand and the protein. The resulting molecules we synthesized were dopamine and serotonin modified at the hydroxyls with a thiol-terminating polyethylene glycol (PEG) chain, or mercaptopolyethylene glycol

dopaminyl ether (MEGaDEth, 1) and mercaptopolyethylene glycol serotonyl ether (MEGaSEth, 2) (Scheme 2), respectively.

The synthesis of the dopamine analog is outlined in Scheme 3. The primary amine of dopamine was protected using di-*tert*-butyl dicarbonate in a previously described method[114] to yield the protected monoamine 3. Both hydroxyls of the PEG chain were replaced by bromine using phosphorus tribromide,[115] resulting in a bromo-PEG-bromide 4. A trityl-protected thiol was introduced onto one end of the PEG chain by reacting 4 in excess with tripheylmethanethiol,[115] giving 5. The protected final product 6 was obtained by substitution of the remaining bromide on 5 with the BOC-protected monoamine 3. Treatment of 6 with a trifluoroacetic mixture removed both protecting groups to give the final desired product 1. The same set of reactions were carried out to make the serotonin analog 2 starting with *N,N*-di-BOC serotonin obtained commercially.

The ligands were conjugated to pcLCIO by mixing the two components together at ratios of 1000 to 2000 ligands per nanoparticle. While the exact number of ligands that can be conjugated per nanoparticle is uncertain due to assay sensitivity limitations and signal interference from nanoparticles, we estimate that there are ~100 ligands per nanoparticle based on the number of DNA oligomers that can be conjugated under the same conditions. Conjugation of ligand to the nanoparticles was confirmed by running modified nanoparticles and unmodified nanoparticles in a 0.5% agarose gel by electrophoresis. Nanoparticles that are successfully coated with ligand should exhibit a more positive surface charge due to the amine groups and therefore migrate a shorter distance down the gel compared to the unmodified nanoparticles.[116] Nanoparticles modified with 0, 1000, and 2000 ligands per pcCLIO ran from the longest to shortest distance, respectively, on the agarose gel.

## BM3h mutagenesis for higher MEGaDEth affinity

MEGaDEth was titrated onto 9D7.S450C and the $K_d$ was determined to be 108 ± 2 μM, which was significantly lower than the affinity for dopamine, which 9D7.S450C binds with $K_d$ of 2.6 ± 1.4 μM. With such low binding affinity, aggregation dynamics of the nanoparticles may be very slow or even thermodynamically prohibitive to clustering. Consequently, mutations were made to 9D7.S450C to improve the ligand binding affinity. The crystal structure of dopamine-bound 9D7[108] was examined to identify amino acid side groups to modify. Using UCSF Chimera and the Build Structure feature, a PEG chain was added to the *para* hydroxyl of dopamine to identify side chains that could be sterically hindering the linker (Figure 1a). The amino acid residues L17 and Q189 were identified as candidates to modify. The mutations L17A, Q189S, Q189T, and combinations of these mutations, were introduced into 9D7.S450C via site-directed mutagenesis. These amino acid substitutions were intended to shorten the side chain to prevent steric clash between the ligand PEG chain and the protein while conserving the charge in order to minimize the impact of the mutations on the protein structure. Preserving the protein structure would likely reduce any impact on the dopamine binding affinity. Titrations with MEGaDEth showed that all of the mutants had significantly improved affinities for the ligand, with $K_d$ values lower than of 9D7.S450C by an order of magnitude (Figure 1b). Additionally, the mutations did not perturb the dopamine binding affinity, possibly due to the conservative nature of the mutations and the relatively large distance between the mutated residues and the active site. Previously, mutations outside of the active site have been shown to have little change on the binding affinity and selectivity compared to the parent BM3h variant.[108]

Unlike 9D7.S450C, 2G9C6.S450C bound MEGaSEth with similar affinity to serotonin.

The MEGaSEth $K_d$ was estimated to be 2.4 ± 1.2 µM from the thiol-oxidized compound. While the thiol is necessary for conjugation, the molecule could still bind to the protein because only the primary amine coordinates with the protein heme group. Since the binding affinity for the tethered ligand was comparable to that of serotonin, no additional mutations were made to 2G9C6.S450C. The difference in tethered ligand binding between 9D7.S450C and 2G9C6.S450C is likely related to the different binding orientations of dopamine and serotonin in these proteins, respectively. The hydroxyindole group of serotonin points in an alternative conformation compared to the dopamine aromatic ring,[108] possibly altering accessibility of the PEG linker to the binding pocket.

**Conditions for aggregation**

A model was developed to query the effect of immobilized ligand-BM3h binding affinities and the density of nanoparticle functionalization on aggregate formation. In the model, we vary the number of proteins and ligands bound on nanoparticles, and determine the percentage of ligand binding sites that would be occupied for a given binding affinity. The geometry of the system is accounted for by considering protein-ligand interactions at surface interfaces that are possible given the curvature of the spherical nanoparticles. At the interface where proteins and ligands may interact, we modeled binding under the assumption that avidity effects are possible, where high local concentrations of immobilized ligand could facilitate multiple protein-ligand interactions and consequently enhance the apparent affinity between nanoparticles. The model outputs the fraction of binding sites that would be occupied at equilibrium. We used to the model to scan a range of total protein and ligand concentrations, and $K_d$ of individual protein-ligand interactions to examine whether system conditions would allow aggregates to form. For the

dopamine and serotonin sensors, we used $K_d$ values of 15 µM and 2 µM in the model, respectively. The model output is shown in Figure 2.

The nanoparticles can be coated with up to 80 BM3h per core, which corresponds to $10^{-7}$ M protein when 1 nM of nanoparticles are used, as set in the model. Similarly, we have $10^{-7}$ M ligands when nanomolar amounts of nanoparticles for our estimate of 100 ligands per pcLCIO. The model predicts that for both sensors, upwards of 90% of sites can be occupied at equilibrium when both total protein and ligand concentrations are ~$10^{-7}$ M and the nanoparticle species are mixed at equimolar ratio. This model indicates that nanoparticle crosslinking via protein-ligand interactions is possible with the binding affinities our ligands have for BM3h. However, the model does not provide information regarding the size of the clusters that can form.

In addition to binding affinity, the ratio of receptor to ligand is an important factor for aggregate formation.[21,113] If the ratio is too low, then the binding sites may be saturated without any crosslinking interaction. If the ratio is too high, then there may be an insufficient number of protein-ligand binding interactions for aggregation. A model system using biotinylated BM3h-9D7 and streptavidin was used to investigate the conditions required for aggregate formation. In this system, BM3h-9D7 was biotinylated at a ratio of 3 biotin molecules per protein molecule then conjugated to SPIO. Varying amounts of streptavidin were added to the nanoparticles until aggregation could be detected using dynamic light scattering (DLS) and MRI. In this system, aggregation occurred when the number of biotin binding sites to biotin was approximately 0.5:1, respectively. At ratios higher or lower, aggregation could not be observed with either detection method (Figure 3). Notably, the $T2$ relaxation of the aggregated nanoparticles was approximately twice that of the dispersed nanoparticles, at 9.36 s$^{-1}$ compared to 4.65 s$^{-1}$, resulting in darkening of the MR image (Figure 3). The biotin concentration and correspondingly, the BM3h-9D7

concentration were relatively low, at 0.41 μM and 0.14 μM, respectively. This protein concentration is significantly lower than the amount of protein alone required for imaging (~$10^{-6}$ M for *in vitro* and *in vivo* imaging).[18,108–110] While the $K_d$ between biotin and streptavidin is on the order of $10^{-14}$ M, much stronger than that of BM3h and any of the neurotransmitters, this model system still indicates that the nanoparticle mechanism can significantly reduce the concentration of sensor required and favour nanoparticle aggregation even under conditions where BM3h and MEGaDEth concentrations are substantially below the $K_d$ of their biomolecular binding interaction.

## 2.3    Conclusions

Our results indicate that coupling BM3h-based sensors to superparamagnetic nanoparticles can improve the potency of the contrast agent, greatly reducing the concentration needed for imaging and physiological effects that accompany it. Aggregation of streptavidin and pcLCOs modified with biotinylated BM3h indicated that a *R2* signal change of up to 80 ± 28% is possible between the aggregated and disaggregated states. The concentration of BM3h in the system was only 0.14 μM, which was about two orders of magnitude lower than the concentration required for *in vivo* imaging using BM3h alone. We have synthesized PEGylated dopamine and serotonin which bind 9D7 and 2G9C6, respectively, with affinities that are high enough to produce interparticle interactions as determined by modeling. These tethered ligands on pcLCIOs should be mixed with BM3h-pcCLIOs to determine ratios of the two components that are needed to produce aggregates that are detectable with DLS and MRI. Aggregate formation should also be confirmed visually by a microscopy method such as atomic force microscopy (AFM) or electron

microscopy (EM). Dopamine or serotonin should also be titrated onto the sensor aggregates to evaluate the sensitivity of the mechanism using both DLS and MRI. Sensitivity at sub-physiological concentrations would allow broader applicability of the BM3h sensors in *in vivo* studies. For example, the nanoparticle-based serotonin sensor could be used to elucidate serotonin release pathways rather than being limited to serotonin reuptake studies. The nanoparticle disaggregation system could also serve as a platform for creating sensors for other small molecules that are ligands for other proteins.

## 2.4   Methods and Materials

### Site-directed mutagenesis of BM3h-9D7

Mutations were introduced using the Agilent QuikChange Lightning Multi Site-Directed Mutagenesis kit (Agilent, Santa Clara CA). The parental plasmid, pCWori cytochrome P450-BM3h 9D7, can be obtained from Addgene (Plasmid #61308). Mutagenesis primers were designed using the QuikChange Primer Design online tool and polymerase chain reaction (PCR) mixtures and thermal cycling were set up according to the manufacturer protocol. The PCR extension time for pCWori BM3h was 3.25 minutes. Parental DNA was removed by digestion with *Dpn* I restriction enzyme supplied in the kit. XL10-Gold competent cells were transformed with *Dpn* I-treated DNA from the mutagenesis reactions and plated onto Luria Broth (LB) agar plates with 100 μg/mL carbenicillin for selection.

**Expression and purification of recombinant BM3h proteins**

BM3h proteins were expressed and purified following methods previously described.[18] Briefly, BM3h plasmids were transformed into BL21(DE3) *E. coli* cells (Thermo Fisher Scientific, Waltham MA). Colonies were incubated overnight in terrific broth (TB) containing 100 µg/mL carbenicillin at 30°C in a shaking incubator. Overnight cultures were diluted 1:100 in TB with 100 µg/mL carbenecillin and incubated at 37°C with shaking until the cultures were induced at late log phase (OD600 ≈ 0.8 – 1.0) with 1.0 mM isopropyl β-D-1-thiogalactopyranoside (IPTG) and 0.6 mM of the heme precursor δ-aminolevulinic acid. Cultures were shaken for an additional 18-24 h at 30°C. The cells were then pelleted and lysed using Bugbuster with lysonase and an EDTA-free protease inhibitor cocktail set (EMD Millipore, Billerica MA) diluted 1:200. BM3h was affinity purified from the soluble fraction of the lysate using Ni-NTA agarose (Qiagen, Germantown MD). The eluted protein was desalted and exchanged into phosphate buffered saline (PBS) over G-25 sephadex columns (GE Healthcare Life Sciences, Marlborough MA). Protein concentration was determined using a carbon monoxide binding assay.[117]

**Ligand titrations onto BM3h**

Ligand binding affinities of BM3h variants were determined from spectrophotometric readings of titration series in a microtiter plate, similar to the method previously described.[18] BM3h at 1 µM in PBS was mixed with ligand solutions freshly prepared in double deionized water (ddH2O) at a range of concentrations. Absorbance spectra were read from the wells from 340 nm – 460 nm at 2 nm intervals at room temperature (Spectramax Plus, Molecular Devices, Sunnyvale CA). To calculate the $K_d$, first the difference spectra were generated by subtracting the signal from the ligand-free protein. The differences between the maximum and minimum of the difference

spectra were calculated and plotted against the ligand concentration. $K_d$ values were determined by fitting a single site ligand depletion binding model to the sigmoid plot.


**Preparation of photocrosslinked lipid coated iron oxide nanoparticles (pcLCIO)**

Iron oxide nanoparticle cores were coated with lipids for solubility and stability in physiological buffers, and functionalization for conjugation using a previously described method.[113]The lipid used was 1,2-bis(10,12-tricosadiynoyl)-*sn-glycero*-3-phosphoethanolamine-N-[maleimide(polyethylene glycol)-2000], which has photo-crosslinking alkyne, PEG2000, and maleimide groups (product #791127, Avanti Polar Lipids, Alabaster AL). Lipids and 10 nm iron oxide cores (Ocean Nanotech, San Diego CA) were mixed at a ratio of 45 mg lipid: 1 mg iron in 300 μL-350 μL of chloroform. The mixture was sonicated for 1 minute. The solvent was thoroughly removed by rotovap drying. The nanoparticles were resuspended in 10 mM Tris 150 mM NaCl buffer pH 6.8, sonicated for 1 minute, and transferred to a 1 mm thick glass cuvette (Starna Cells, Atascadero CA). Argon gas was bubbled into the nanoparticle solution for 10 minutes to purge oxygen. The solution was UV irradiated at 254 nm for 45 min for the lipids to crosslink around the iron cores. The resulting pcLCIO were purified over magnetic columns (Miltenyi Biotec, San Diego CA) into PBS to remove micelles and empty liposomes. Maleimide functionalized particles were used the same day they were prepared.

To prepare ligand-coated pcLCIO, the ligands were first reduced with tris(2-carboxyethyl)phosphine (TCEP) at a molar ratio of 1:1 for 4 h at room temperature. Without removing TCEP, the ligand was added to pcLCIO at ratios ranging from 1000:1 to 2000:1 ligands per nanoparticle, respectively. The ligand concentration ranged from 0.3 mM-0.6 mM, with the nanoparticle concentration at 300 μM. The mixtures were incubated overnight at room

temperature. The iron concentration should be $\geq 5$ mM in the reaction mixture. Unreacted ligand was removed by washing and filtration using 100 kDa molecular weight cut off spin filters (EMD Millipore). To determine whether pcLCIO were successfully modified with ligand, samples of unmodified pcLCIO and ligand-pcLCIO were analyzed using agarose gel electrophoresis. At least 4 ng iron of each sample was loaded onto a 0.5% agarose gel and run in tris-acetate-EDTA (TAE) buffer. Ligand-pcLCIO should migrate further down the gel, with the distance dependent on the degree of modification.

BM3h-pcLCIO were prepared by incubating BM3h with pcLCIO at a molar ratio of 1000:1, respectively, overnight at 4°C. The reaction was purified over a magnetic column into PBS to remove unreacted protein. The protein concentration on the pcLCIO was determined using the Pierce 660 nm protein assay (Thermo Fisher Scientific), using bovine serum albumin (BSA) mixed with pcLCIO as standards.


**Light scattering experiments**

Dynamic light scattering (DLS) measurements were taken using a DynaPro DLS system (Wyatt Technology, Goleta CA) at 25°C with averaging over 100 acquistions and 1 s integration time. The laser power was set at 20%. pcLCIO samples were prepared at 100 μM Fe and 20 μL of sample was used for each measurement.


*In vitro* **magnetic resonance imaging**

Samples for MRI were prepared at 100 μM Fe, with 40-50 μL of the sample loaded a 384-well microtiter plate. Wells that did not contain any samples were filled with the same volume of PBS. Imaging was performed with a 20-cm-bore Bruker 7 T MRI scanner at room temperature.

A 2 mm slice through the sample was imaged using a $T2$-weighted multi-spin multi-echo pulse sequence; repetition time ($TR$) was 2 s, and echo time ($TE$) ranged from 12-32 ms at 4 ms intervals. Custom MATLAB routines were used to reconstruct and analyze images, and calculate $T2$ relaxation rates by exponential fitting to the image data, using the equation $I = k\exp(-TE/T2)$, where $I$ was the MRI signal intensity and $k$ was a constant of proportionality.

**tert-butyl (3,4-dihydroxyphenethyl)carbamate**

Dopamine hydrochloride (1 g, 5.27 mmol) was mixed with di-*tert*-butyl dicarbonate (1.34 mL, 5.83 mmol) at approximately 1:1 molar ration in approximately 12 mL of a solution of tetrahydrofuran (THF) and saturated $NaHCO_3$. The reaction was stirred for 2 h at room temperature under argon. The resulting solution was extracted with 50 mL of ethyl acetate (EtOAc) with 3 mL of $H_2O$, recovering the organic layer. The extraction was repeated to recover more material. The organic layers were combined and dried over $MgSO_4$, and the solvent was removed *in vacuo*.

**1-bromo-2-(2-(2-(2-bromoethoxy)ethoxy)ethoxy)ethane**

PEG was dissolved in anhydrous dichloromethane (DCM) and 2 molar equivalents of $PBr_3$ were added. The reaction mixture was stirred overnight at room temperature. The solvent was removed *in vacuo* and the resulting oily residue was redissolved in hexane. The organic solution was washed carefully with saturated $KHCO_3$ twice, collecting the organic layer. The organic layer was then extracted twice with saturated NaCl, again recovering the organic layer. The recovered solution was dried with $MgSO_4$, filtered, and dried *in vacuo*.

## 13-bromo-1,1,1-triphenyl-5,8,11-trioxa-2-thiatridecane

Di-bromo-PEG, tripheylmethanethiol, and K2CO3 were mixed at molar ratios of 3:1:0.5 in anhydrous dimethylformamide (DMF), first dissolving the di-bromo-PEG then adding the other material. Reaction was stired overnight with reflux at 80°C. The solvent was removed by rotovap and the oily residue remaining was suspending in a 50/50 vol/vol% solution of water and acetonitrile then injected into reverse phase HPLC with C18 column. The desired product eluted at 80% acetonitrile.

## tert-butyl(3-hydroxy-4-((1,1,1-triphenyl-5,8,11-trioxa-2-thiatridecan-13-yl)oxy)phenethyl)carbamate

The reaction flask is purged with argon before adding reaction materials. Boc-monoamine and $K_2CO_3$ were dissolved at molar ratio of 1:0.5 in dry DMF, and mixed for 15 min at 80°C under argon. Di-bromo-PEG was added to the reaction mixture at a 1:1 molar ratio to the boc-monoamine. The solution was mixed overnight at 80°C under argon. The solvent was removed by rotovap, leaving an oily residue which was purified by flash chromatography. The silica was equilibrated in 50:50 vol/vol% hexane/EtOAc. The oily residue was dissolved in the same solvent mixture and loaded directly onto the column silica. The eluent was 50:50 vol/vol% hexane/EtOAc mixture. UV-active fractions that were verified to be our product by thin liquid chromatography (TLC) on silica plates were collected, pooled, and dried *in vacuo*.

## 5-(2-aminoethyl)-2-(2-(2-(2-(2-mercaptoethoxy)ethoxy)ethoxy)ethoxy)phenol

The purified product was deprotected with a mixture of 90 vol% TFA, 1 vol% triisopropyl silane, 1 vol% H2O, and 8 vol% methanol. The compound was dissolved in this solution at ~50

mg/mL. The mixture was incubated at room temperature with shaking for 2 h. The solvent was removed by blowing a stream of air over the mixture. The dried material is resuspended in methanol and filtered to remove the white precipitate that formed during deprotection. The solvent is removed by rotovap. The final product is recovered by reverse phase HPLC purification with a C18 column, where the product eluted at 55% acetonitrile.

**Free dopamine**

High relaxivity                    Low relaxivity
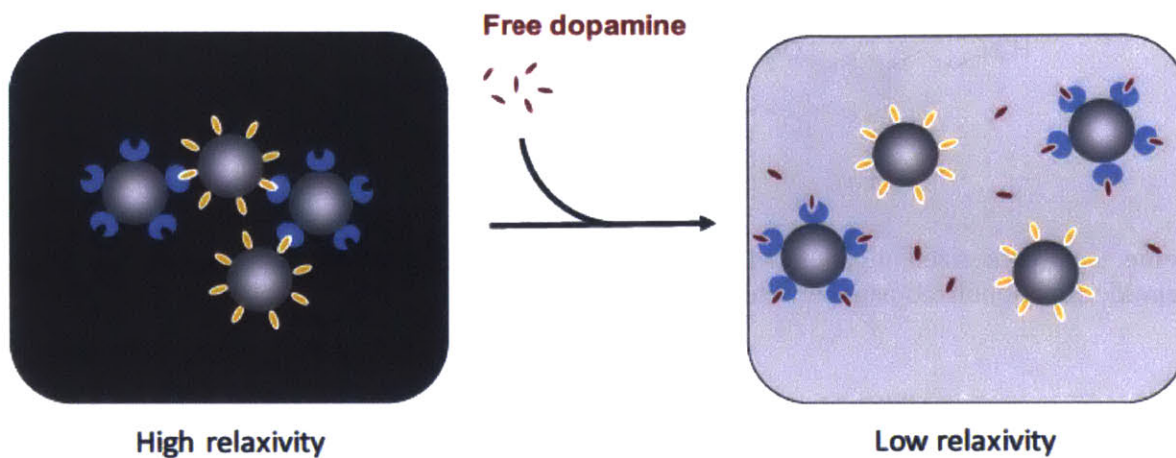
**Scheme 1.** Preformed clusters of nanoparticle species coated with BM3h (blue) and dopamine (yellow) disperse upon addition of free dopamine (red) to the system, competing for the binding sites on BM3h which results in disaggregation of the clusters.
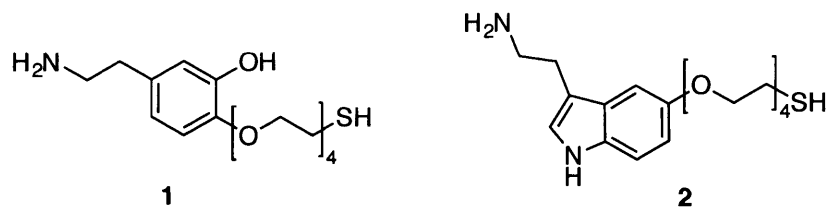
**Scheme 2.** Synthesized ligands MEGaDEth **(1)** and MEGaSEth **(2)** for conjugation to maleimide-functionalized nanoparticles.
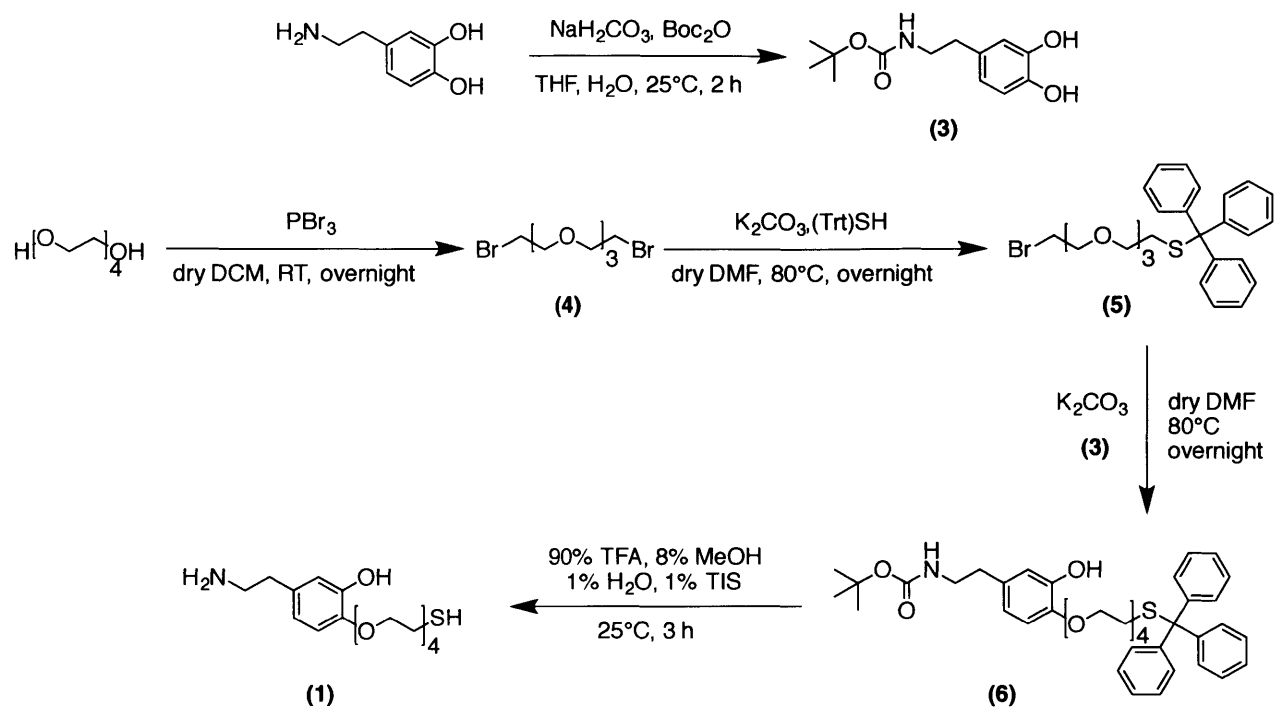
**Scheme 3.** Synthesis of MEGaDEth **(1)** starting with tetraethylene glycol and dopamine.
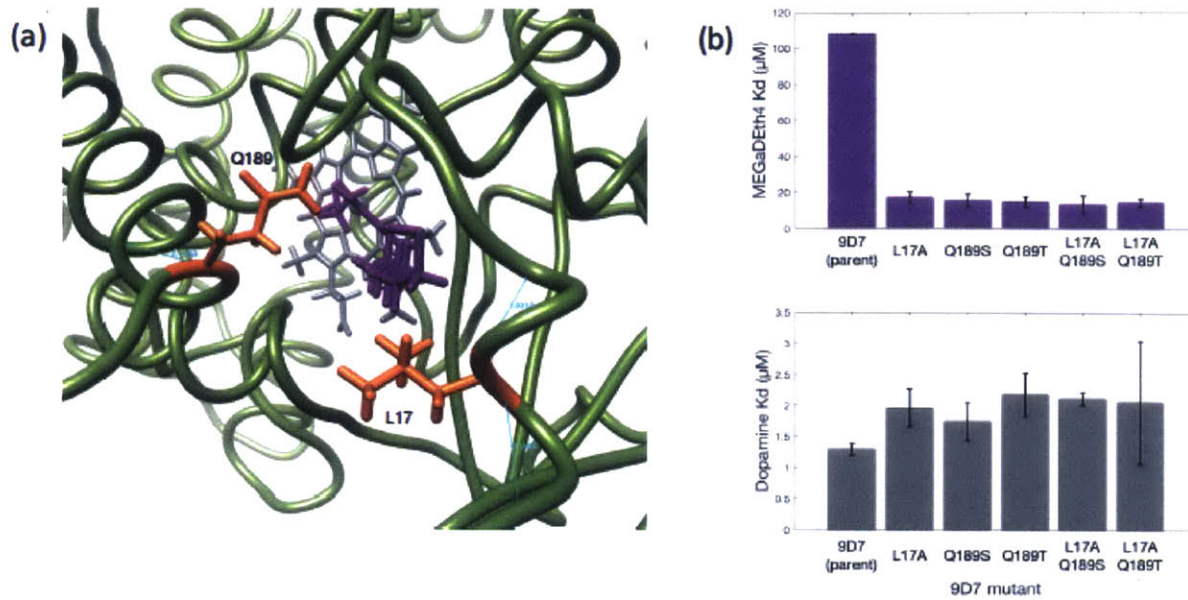
**Figure 1.** 9D7 mutations to improve protein binding affinity for MEGaDEth. (a) Crystal structure of dopamine-bound 9D7[108] (green backbone) with modeled PEG linker (purple) used to identify sites for mutation, L17 and Q189 (orange). (b) Comparison of MEGaDEth (purple) and dopamine (grey) dissociation constants of mutants compared to 9D7. Errors are reported as standard deviations for $n = 3$.
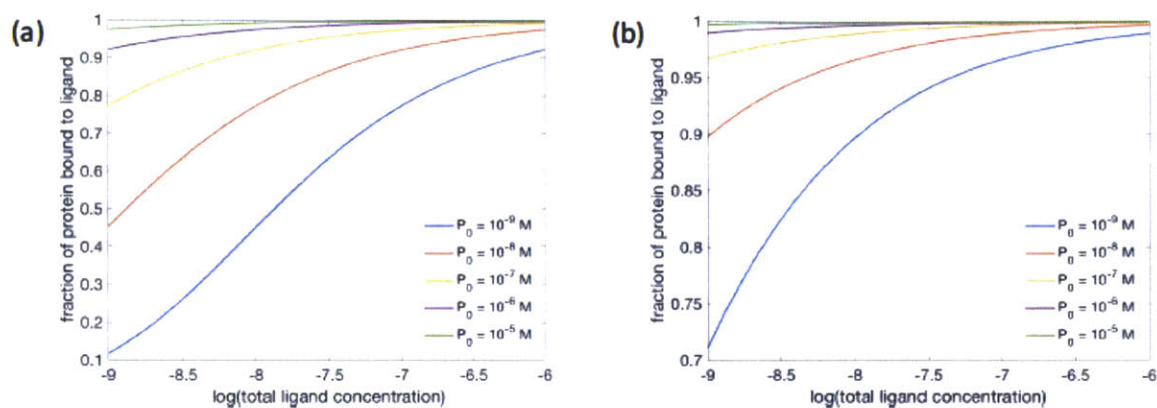
**Figure 2.** Model output when nanoparticle species are mixed at molar ratio of 1:1 with 1 nM of each nanoparticle species and assuming avidity effects. $P_0$ is the total initial protein concentration. The model resultsindicate that (a) > 70% of protein sites will be occupied for $K_d$ = 15 μM, and (b) > 95% for $K_d$ = 2 μM for total ligand concentration of $10^{-7}$ M.
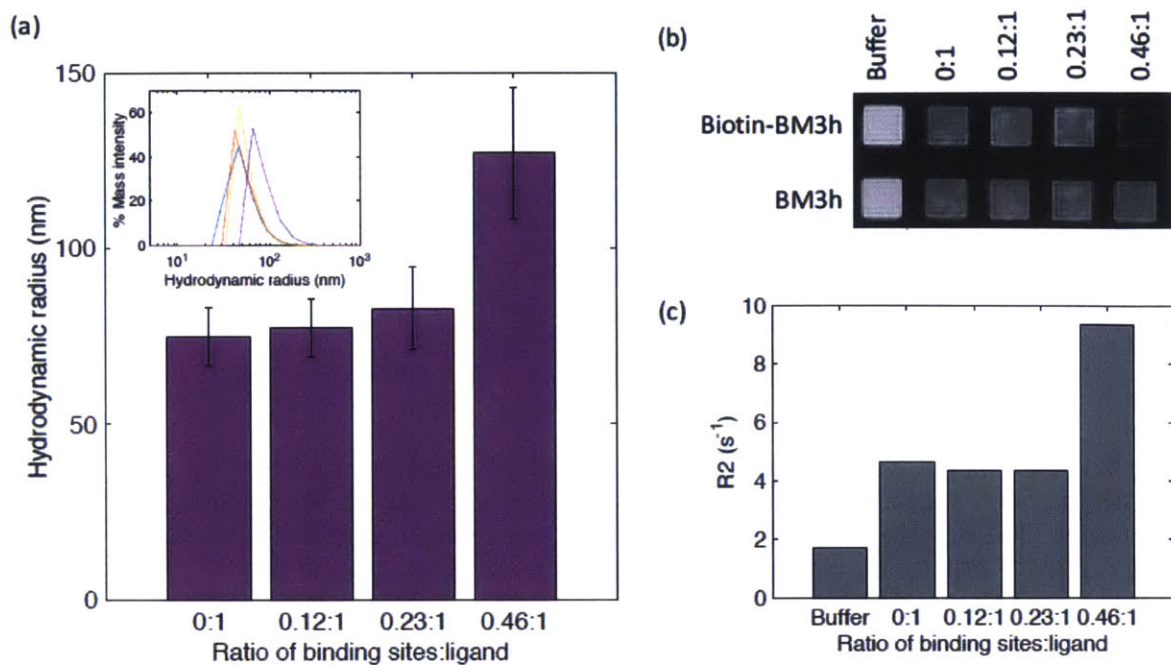
**Figure 3.** Biotinylated-BM3h-pcLCIO and streptavidin model system only showed aggregation when the ratio of biotin binding sites to biotin was 0.46:1, respectively. (a) Hydrodynamic radius as determined from DLS showed two-fold increase in the cluster size for 0.46 sites:1 biotin sample of streptavin-pCLIO and biotinylated BM3h-pcLCIO mixtures compared to unclustered nanoparticles. Inset shows the DLS histogram results of the same mixtures, where blue is 0 sites: 1 biotin, red is 0.12 sites: 1 biotin, yellow is 0.23 sites: 1 biotin, and purple is 0.46 sites: 1 biotin. (b) *T2*-weighted images of samples obtained at 7 T, room temperature. Biotin-BM3h samples contained pcLCIO coated with biotinylated 9D7, BM3h samples contained pcLCIO coated with 9D7 without biotin. Buffer samples do not contain any nanoparticles. All samples with nanoparticles contain 100 μM total iron concentration. (c) *T2* relaxation rates of biotin-BM3h samples in panel b measured at 7 T, room temperature.

# 3 Semi-rational design of a high relaxivity metalloprotein from phenylalanine hydroxylase

## 3.1 Introduction

Magnetic resonance imaging (MRI) can be used for molecular imaging non-invasively and with high spatial resolution through the administration of contrast agents. Contrast agents are substances that can enhance the signal of particular physiological features, allowing better signal to noise ratios and shorter imaging times. In clinical structural MRI, synthetic gadolinium complexes are the most commonly used contrast agents. The development of these agents has focused largely on gadolinium because it has the most unpaired electrons of any ion and relatively slow electronic relaxation rate, giving rise to its high relaxivity in MRI. The relaxivity of Gd(III) complexes is mostly due to the interactions between the ion electron spins and water protons in the primary coordination sphere of gadolinium, known as inner sphere effects. Solomon, Bloembergen, and Morgan developed a set of equations, the SBM equations, that describe the mechanism and contribution of various parameters to inner sphere relaxivity.[4] We know from these equations that one of several possible ways to tune Gd(III) complexes for higher relaxivity is to elongate the rotational correlation time, $\tau_R$, by developing a high molecular weight system. This approach is often executed by coupling the metal complex with a protein or other macromolecule, such as human serum albumin (HSA), and has demonstrated that remarkable increases in relaxivity are possible.[118]

Direct coordination of lanthanides to a macromolecule has been investigated primarily through substitution of lanthanides into native calcium-binding sites,[119–121] incorporation of

synthetic lanthanide chelators or unnatural amino acids into protein backbones,[122] and the development of lanthanide binding tags (LBT).[123–125] These efforts have largely produced peptides targeted for terbium and europium binding to produce tools for studying protein structure, protein-protein and protein-ligand interactions, with evidence that some of these peptides are MRI active when bound to gadolinium.[126,127] Peptides, however, lack the tertiary structure typically needed for small molecule recognition and binding. To produce a lanthanide-bound biomolecule capable of sensing for molecular imaging, a protein complex would be needed.

We investigated the use of semi-rational protein engineering to design an MRI-visible protein capable of binding lanthanides that could eventually be tuned for monoamine neurotransmitter binding using a native protein scaffold. Semi-rational design of proteins allows for screening of smaller libraries through selection of specific target sites and mutations, reducing the screening effort and allowing the use of analytical methods that are not typically compatible with high-throughput screening. Phenylalanine hydroxylase (PAH) from *Chromobacterium violaceum* was chosen as the starting native protein scaffold because it naturally chelates a metal ion that shows coordination with catecholamines. PAH is a non-heme iron enzyme that catalyzes the hydroxylation of phenylalanine to tyrosine. Its structure and kinetic properties have been broadly studied due to its role in phenylketonuria, a genetic disorder that affects phenylalanine metabolism.[128,129] PAH activity is known to be inhibited by catechol binding in the active site, possibly as part of a regulatory pathway for catecholamine synthesis. Catecholamines including epinephrine, norepinephrine, and dopamine have been shown to act as allosteric inhibitors that bind with $K_d$ measurements ranging from nanomolar to sub-millimolar.[130–133] These ligands bind through coordination of the catecholic hydroxyls with the

active site iron ion, which crystal structures have shown causes displacement of two iron-coordinated water molecules,[134] suggesting that it could produce ligand-dependent MRI signal changes. We designed a library of 16 mutants and a fluorescence assay for measuring gadolinium binding affinities through which we identified mutations that improved gadolinium binding affinity and relaxivity that could be further engineering to be a suitable molecular imaging agent.

## 3.2 Results and discussion

**Rational mutant library design**

Our goal was to tune the existing metal-binding site of PAH for higher binding affinity to gadolinium. Existing PAH crystal structures[134,135] were examined to identify amino acid modifications that could be made to produce a more negatively charged binding pocket that would favour gadolinium binding. The iron in PAH is coordinated by 3 residues: H138, H143, and E184, in an arrangement known as the 2-His-1-Glu motif that is common in mononuclear non-heme iron enzymes.[136] The remaining coordination sites of the iron are occupied by water molecules in the absence of a ligand. For the library, the histidine iron-coordinating residues were mutated to the negatively charged residues aspartate or glutatmate. The negatively charged oxygen atoms of the carboxylate groups of these amino acids are the preferred donor atoms of gadolinium.[137] In peptide structures containing lanthanides, the majority of metal coordination ligands are carboxylate groups.[120] E184 was not modified in part because it is known to form a hydrogen bond to the hydroxyl of a bound catecholamine.[134]

With the native metal-coordinating glutamate residue and the mutated histidine residues, the metal binding site has a total of 5-6 possible donor atoms. In solutions of physiological pH, gadolinium has large coordination numbers of 8-10 and typical synthetic ligands have eight donor atoms[120,137] while protein binding of gadolinium involves an average of 5.9 coordination atoms.[120] To explore the effect of high coordination site numbers on PAH lanthanide binding, mutations were made to amino acids outside of the iron-binding triad in order to provide additional donor atoms. The residues P134 and A199 were selected for mutation based on their proximities to the metal binding site as determined from crystal structures and by the possible aspartate and glutamate rotamers as determined using the UCSF Chimera Rotamer tool (Figure 1). Again, these residues were mutated to either aspartate or glutamate to incorporate more negatively charged oxygen donor atoms. Sixteen point mutants in total were created with the described mutations using site-directed mutagenesis, 8 of which expressed properly in *Escherichia coli*. The protein yields of the mutants varied great from 18 mg/L to 71 mg/L. By comparison, the wild type protein can be expressed at levels of approximately 55 mg/L (Table 1) indicating that some mutations were destabilizing.

**Effect of Mutations on PAH Gadolinium Binding Affinity**

To assess the effects of the mutations on gadolinium binding, we developed a competition assay based on the lanthanide-sensitive fluorophore Fluo-4 to measure the binding affinity of the mutants. In this assay, apo-PAH was titrated onto preformed $Gd^{3+}$-Fluo-4 complex. If the protein is able to sequester gadolinium from the fluorophore complex, then the fluorescence is progressively quenched with higher protein concentrations (Figure 2). The protein $K_d$ for

gadolinium was obtained by fitting the equation for one-site competitive binding to the data with the $K_d$ of Fluo-4 for gadolinium set as 94 nM, as determined from our measurements.

Remarkably, all of the expressed mutants in our library showed a higher affinity for gadolinium than the wild type, as determined by the fluorescence competition assay (Table 1). This indicates that generally producing a more negatively charged binding pocket does improve gadolinium binding, presumably to accommodate the higher positive charge of the ion. Wild type PAH was found to bind gadolinium with $K_d$ of 29.2 ± 4.0 μM and the mutants with the most improved affinities, P134D and P134D H138D, had $K_d$ values of 0.58 ± 0.06 μM and 0.64 ± 0.32 μM, respectively. Both mutants contain the P134D mutation, suggesting that this additional metal coordination site is sufficient for achieving submicromolar binding affinities. The $K_d$ of the H138D mutation alone was 4.3 μM. While this was an order of magnitude improvement in the binding affinity compared to wild type, the double mutant indicates that the two mutations were not synergistic. P134D H138D also indicates that more coordination sites do not necessarily lead to higher binding affinity, as the double mutant could provide up to 7 coordination atoms while the single mutant can provide up to 6 coordination atoms. The difference may be attributable at least in part to differences in coordination geometry. The preferred geometry of gadolinium in solution with coordination number of 8 is a square antiprism[137] and binding is likely improved in geometries that more closely approximate this configuration. The additional donor atoms introduced by the mutations also do not necessarily participate in gadolinium coordination. The replacement of the conformationally-restricted proline by aspartate may add beneficial flexibility to the binding site, allowing the binding pocket to be more accommodating to the larger ion gadolinium.

Another mutation to the same site, P134E, resulted in a PAH variant with gadolinium $K_d$ of 4.5 μM. The side chain of an aspartate residue is shorter than that of a glutamate residue and different orientations of the carboxylate group as a result, factors which could both contribute to a lower binding affinity. Mutants with A199D mutations also did not show as significant changes in $K_d$ compared to the P134D mutants (Table 1). Only double mutants of A199D were expressed and their binding affinities were lower compared to those of their single mutation counterparts, suggesting that A199D does not contribute to gadolinium binding. The results of P134E and the A199D double mutants corroborate the conclusion that not all additional ligand coordination sites can improve gadolinium binding to the same extent and that other factors such as coordination geometry need to be considered in addition to increasing the number of negatively charged donor atoms. The geometry of metal binding could be better examined and improved using computational methods that can compare and model designs based on existing calcium binding sites in proteins,[138,139] such as the *E. coli* receptor for D-galactose and D-glucose, GGR, which was shown to have submicromolar $K_d$ for $Yb^{3+}$ and $Lu^{3+}$.[140]

**Effect of Mutations on PAH Relaxivity**

The proteins were imaged using MRI at 7 T field strength to evaluate the effects of the mutations on longitudinal relaxivity. For the measurements, solutions of each mutant were prepared with 150 μM apo-protein mixed with freshly prepared $GdCl_3$ at 80 μM. While all of the mutants exhibited higher gadolinium binding affinity than the wild type, not all of the mutants showed increased relaxivity (Figure 3). Wild type gadolinium-bound PAH had relaxivity of $14.60 \pm 0.03$ $mM^{-1}s^{-1}$ and the only two mutants that showed higher relaxivity were P134D and P134D H138D, with relaxivities of $16.7 \pm 0.2$ $mM^{-1}s^{-1}$ and $17.9 \pm 0.2$ $mM^{-1}s^{-1}$, respectively (Table 1). These

were also the mutants with the lowest $K_d$ values for gadolinium. The remaining mutants all showed relaxivities lower than that of wild type PAH. The seemingly uncorrelated relationship between gadolinium binding and relaxivity could be due to the influence of various factors on relaxivity. The $T1$ relaxivity of complexes of a particular paramagnetic ion is affected by the number of exchangeable water molecules $q$ coordinated with the paramagnetic ion, and the mean residence lifetime $\tau_M$ of the coordinated water molecules. All of the mutants introduced additional potential coordination atoms for gadolinium, which could leave fewer exchange sites for water molecules. Changes to the number of donor atoms can also affect the coordination geometry, possibly altering the water exchange pathways and thus $\tau_M$. Mutants with lower relaxivity that bind gadolinium more tightly may still be desirable as the the gadolinium is less likely to dissociate from the protein or undergo transmetallation, reducing toxicity of the imaging agent. Despite some of the mutants having lower relaxivities than wild type, all of them showed greater relaxivity than gadolinium in solution and existing $T1$ agents for monoamine imaging: the BM3h agents which have relaxivities of up to 1.89 mM$^{-1}$s$^{-1}$ [18,108] and gadolinium chemical chelates have relaxivities of up to 5.5 mM$^{-1}$s$^{-1}$ (MS-325)[141] at a field strength of 4.7 T.

Since catecholamine binding to iron-coordinated PAH is known to displace two water molecules,[134] we imaged the PAH mutants in the presence of dopamine to assess ligand-modulated changes in relaxivity. Dopamine was added at 1 mM to the Gd$^{3+}$-PAH preparations and the relaxivity was measured. Wild type PAH with gadolinium showed weak dopamine modulation, with the relaxivity decreasing by only about 7%. P134D showed the greatest change in relaxivity, at 12% decrease. P134D H138D did not show any improvement in relaxivity modulation by ligand binding (Table 1). The double mutant may have one more metal coordination site than P134D, which may preclude dopamine binding as dopamine binds to the

metal ion through interactions of both catecholic hydroxyl groups.[134] Another mutant, H138D A199D, also showed approximately 12% change in relaxivity with 1 mM dopamine. Interestingly, this mutant did not have the greatest improvement in gadolinium binding and has slightly lower relaxivity than WT $Gd^{3+}$-PAH. While these values should be confirmed with repeated measurements, this mutant demonstrates that stronger gadolinium may be dissociated from the protein by ligand binding. The dopamine-modulated relaxivity changes observed *in vitro* with any of the mutants would not be observable *in vivo*, especially not at physiological extracellular dopamine concentrations which at best reach millimolar concentrations in the synapse.[142] Water molecule displacement may be difficult to predict and model as computational methods are still poor at predicting bound water molecules at interfaces and binding sites,[138] necessitating an MRI-based screening step.

## 3.3    Conclusions

We have demonstrated that a semi-rational protein engineering is a viable strategy for generating a high relaxivity metalloprotein using PAH as the starting protein structure. From a small selective library of mutants, we were able to improve the gadolinium binding affinity of the protein substantially by introducing additional negatively charged donor atoms for gadolinium coordination. Improvements in lanthanide binding also resulted in proteins of higher relaxivities in some cases, while others suggested a trade-off may exist between attaining higher binding affinity and higher relaxivity. This study also highlights the benefits of using a semi-rational approach; it allowed us to screen a smaller library compared to typical library sizes using methods such as directed evolution, and permitted the use of an analytical method that is currently not suitable for high-throughput screening. Our approach also indicated that metal

binding in a metalloprotein contrast agent design could be further enhanced by computational methods in rational protein design,[138,139] perhaps eventually improving the binding affinity to single nanomolar $K_d$ that has been achieved in lanthaninde-binding peptide design.[123] Ligand-modulated relaxivity effects, however, are likely still best explored experimentally. Together, rational design and library screening can be an effective strategy towards developing high relaxivity and high sensitivity protein-based MRI contrast agents.

## 3.4   Methods and materials

**Wild type PAH cloning**

Wild type *Chromobacterium violaceum* phenylalanine hydroxylase (CvPAH) was cloned from the genome of the bacteria into a pET expression vector. Freeze-dried *C. violaceum* was obtained from ATCC (Manassas VA) and grown in Luria Broth (LB) without any antibiotic. Genomic DNA was isolated using a bacterial DNA extraction kit (Zymo Research, Irvine CA) and the CvPAH gene was PCR-amplified with *Nde I* and *Xho I* restriction sites on the 5' and 3' ends of the gene, respectively.  PCR product was separated from genomic DNA by gel electrophoresis. CvPAH was cloned into pET-28a (EMD Millipore, Billerica MA) by digesting both the insert and the vector with the restriction enzymes *Nde I* and *Xho I* (New England Biolabs, Ipswich MA) and joining the digested insert and backbone together with a DNA ligase (New England Biolabs). Inserting CvPAH between the *Nde I* and *Xho I* restriction sites in pET-28a added an N-terminal 6x histidine tag and thrombin cleavage site. The resulting plasmid, pET-28a-CvPAH, was transformed into DH5α *E. coli* cells (Thermo Fisher Scientific, Walthan MA) and plated onto LB agar plates with 50 μg/mL kanamycin.

**Site-directed mutagenesis of PAH**

Mutations were introduced using the QuikChange Lightning Multi Site-Directed Mutagenesis kit (Agilent, Santa Clara CA). Mutagenesis primers were designed using the QuikChange Primer Design online tool and polymerase chain reaction (PCR) mixtures and thermal cycling were set up according to the manufacturer protocol. The PCR extension time for pET28a-CvPAH was 3 minutes 5 seconds. Parental DNA was removed by digestion with *Dpn* I restriction enzyme supplied in the kit. XL10-Gold competent cells were transformed with *Dpn* I-treated DNA from the mutagenesis reactions and plated onto LB agar plates with 50 μg/mL kanamcyin for selection.

**Apo-PAH expression and purification**

CvPAH plasmids were transformed into BL21(DE3)pLysS *E. coli* cells (Thermo Fisher Scientific) for expression. Transformations were plated onto LB agar plates with 50 μg/mL kanamycin and 34 μg/mL chloramphenicol. Colonies were incubated overnight in M9 minimal media containing 50 μg/mL kanamycin and 34 μg/mL chloramphenicol at 37°C in a shaking incubator. Overnight cultures were diluted 1:100 in M9 minimal media containing 50 μg/mL kanamycin and 34 μg/mL chloramphenicol and incubated at 37°C with shaking until the cultures were induced at late log phase (OD600 ≈ 0.8 – 1.0) with 1.0 mM isopropyl β-D-1-thiogalactopyranoside (IPTG). Cultures were shaken for an additional 5-7 h at 37°C. The cells were then pelleted and lysed using Bugbuster with lysonase and an EDTA-free protease inhibitor cocktail set (EMD Millipore) diluted 1:200. CvPAH was affinity purified from the soluble fraction of the lysate using Ni-NTA agarose (Qiagen, Germantown MD). The eluted protein was

desalted and exchanged into 50 mM hepes 150 mM KCl pH 7.4 over G-25 sephadex columns (GE Healthcare Life Sciences, Marlborough MA) twice. CvPAH concentration was determined by measuring the absorbance at 280 nm and calculated using the extinction coefficient $\varepsilon^{280}$ = 55,190 M$^{-1}$cm$^{-1}$.[135]

**Fluorescence assays and titrations**

All titration experiments were done in 50 mM HEPES 150 mM KCl, pH 7.4 buffer and used Fluo-4 pentapotassium salt (Molecular Probes, Eugene OR) at 1 µM. To determine the gadolinium affinity of Fluo-4, GdCl$_3$ solutions prepared in double deionized water (ddH$_2$O) were mixed with Fluo-4 at various concentrations up to 100 µM. To measure the gadolinium affinity of proteins, the Gd$^{3+}$-Fluo-4 complex was first formed by mixing equimolar amounts of Gd$^{3+}$ with Fluo-4 then added at 1 µM to protein solutions. CvPAH was added to Gd$^{3+}$-Fluo-4 complex at various concentrations up to 1 mM, if protein expression levels were high enough. Fluorescence spectra were obtained by exciting at 488 nm and reading from 515-550 nm at room temperature (Spectramax Plus, Molecular Devices, Sunnyvale CA). The dissociation constant of Gd$^{3+}$ for Fluo-4 was calculated by fitting the fluorescence data to a one site ligand depletion binding model. The dissociation constant of Gd$^{3+}$ for the CvPAH variants were calculated by fitting the data to a one site competitive binding model.

*In vitro* **magnetic resonance imaging**

Samples for MRI were prepared at 50-100 µM CvPAH, with 40-50 µL of the sample loaded a 384-well microtiter plate. For sample wells with ligands, a concentrated ligand solution was made in ddH$_2$O, added to the appropriate wells, and mixed thoroughly by pipetting. For sample

wells without ligand, ddH$_2$O was added instead at the same volume as the ligand solution. Wells that did not contain any samples were filled with the same volume of hepes buffer. Imaging was performed with a 20-cm-bore Bruker 7 T MRI scanner at room temperature. A 2 mm slice through the sample was imaged using a *T1*-weighted multi-slice multi-echo (MSME) pulse sequence; echo time (*TE*) was 20 ms, and repetition times (*TR*) were 116, 186, 298, 477, 763, 1221, 1953, 3125, and 5000 ms. Custom MATLAB routines were used to reconstruct and analyze images, and calculate *T1* relaxation rates by exponential fitting to the image data, using the equation $I = k[1\text{-exp}(-TR/T1)]$, where $I$ was the MRI signal intensity and $k$ was a constant of proportionality.

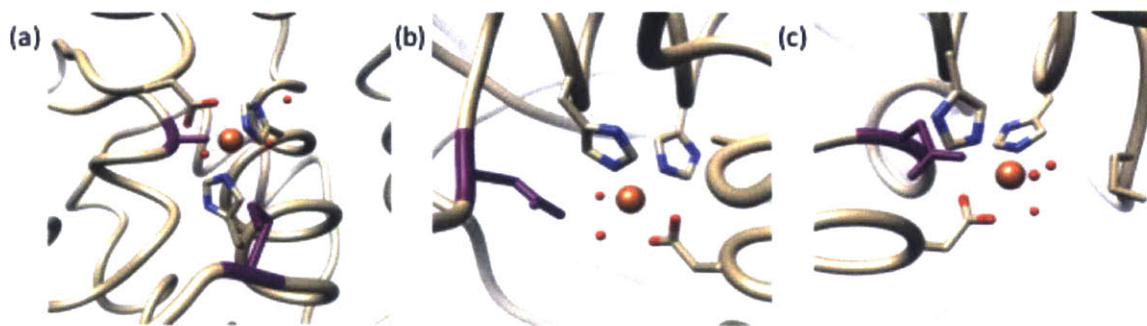**Figure 1.** Residues in PAH mutated to introduce additional gadolinium coordination atoms. (a) Residues A199 and P134 (purple) were identified based on proximity to the metal binding site, and based on the possible rotamers of substitutions. (b) P134D substitution mutation side chain position predicted using UCSF Chimera. (c) A199D substitution mutation side chain position predicted using UCSF Chimera.

**Table 1.** Properties of PAH mutants. Yield obtained from expression in M9 minimal medium and 6xHis tag purification. Gadolinium dissociation constant determined by fluorescence competition assay using $Gd^{3+}$-Fluo-4. $T1$ relaxivity was measured at room temperature at 7 T, normalized to the gadolinium concentration. % change reflects difference between relaxivity of PAH with and without 1 mM dopamine. P134E H143D relaxivity was not measured due to low expression yield.

| Mutations | Yield (mg/L) | Gadolinium Kd (μM) | $T1$ relaxivity (mM$^{-1}$s$^{-1}$) | | |
| --- | --- | --- | --- | --- | --- |
| | | | without ligand | with 1 mM dopamine | % change |
| none (WT) | 55.0 | 29.2 ± 4.0 | 14.60 ± 0.03 | 13.6 ± 0.5 | -6.8 |
| P134E | 54.8 | 4.5 | 9.6 | 9.7 | 1.0 |
| H138D | 51.6 | 4.3 | 10.8 | 11.7 | 8.3 |
| P134D H138D | 52.7 | 0.64 ± 0.3 | 17.9 ± 0.2 | 16.6 ± 0.7 | -7.3 |
| P134E H143D | 18.0 | 1.5 | n/a | n/a | n/a |
| P134E A199D | 42.1 | 4.2 | 10.7 | 9.7 | -9.3 |
| H138D A199D | 67.6 | 7.0 | 13.8 | 12.1 | -12.3 |
| H143D A199D | 71.0 | 10.0 | 13.0 | 11.9 | -8.5 |
| P134D | 66.8 | 0.58 ± 0.1 | 16.7 ± 0.2 | 14.7 ± 0.5 | -12.0 |

Errors shown are standard deviations for n = 3
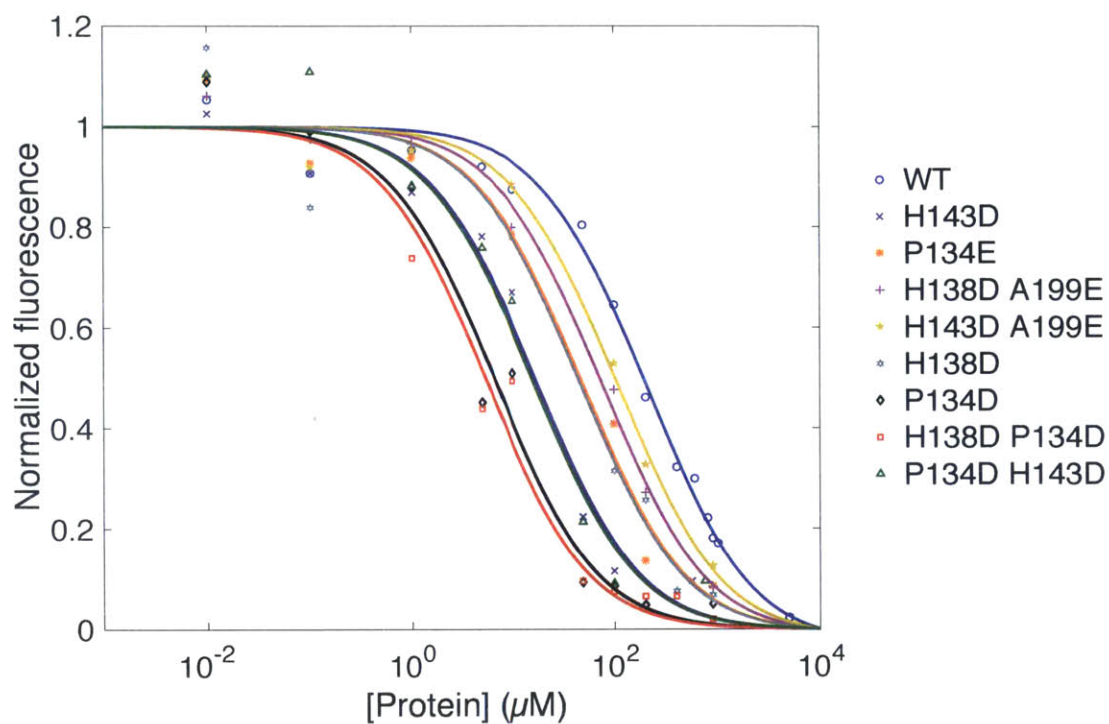
**Figure 2.** Titration of PAH onto $Gd^{3+}$-Fluo-4 results in fluorescence quenching that can be used to determine dissociation constants of the protein variants for gadolinium. All PAH mutants showed improvement in gadolinium binding affinity, with the most improvement seen in mutants P134D and H138D P134D where $K_d < 10^{-6}$ M.

**Figure 3.** Relaxivity of PAH variants without ligand and with 1 mM dopamine measured at 7 T and room temperature. The mutants P134D and H138D P134D were the only mutants that showed improvement in both gadolinium affinity and relaxivity.

# 4 Conclusions and future directions

This thesis described approaches for increasing increasing the sensitivity of contrast agents by coupling ligand sensing with robust signal changes. The first appr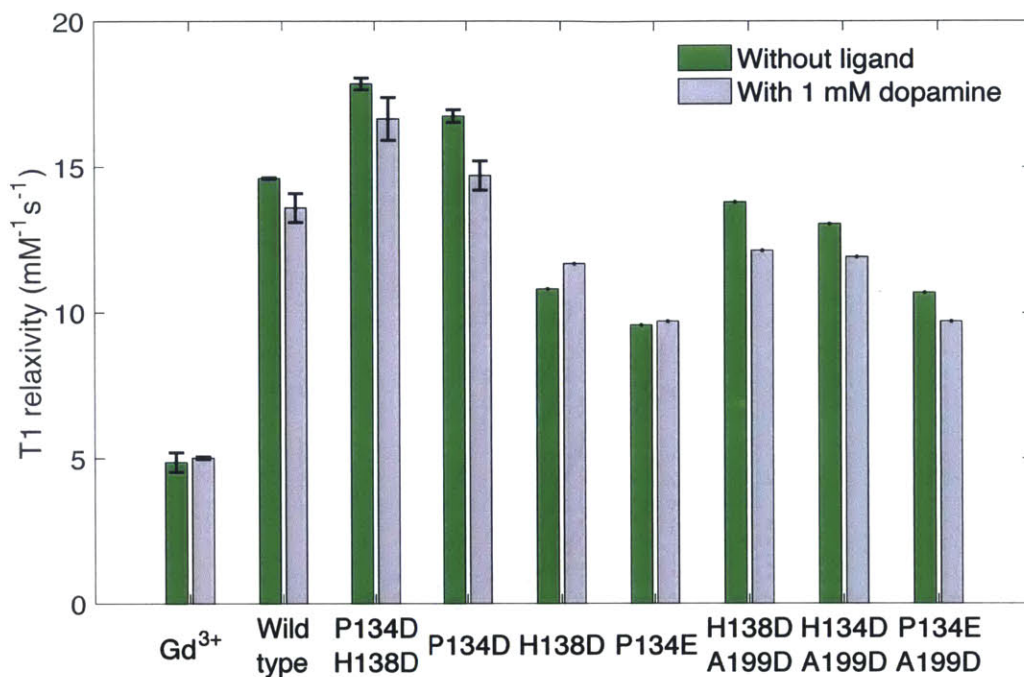oach combined an existing set of protein-based neurotransmitter sensors with superparamagnetic iron oxide nanoparticles to create clusters that disperse in the presence of neurotransmitters. There have been previous sensors which make use of ligand- or enzyme activity-dependent aggregation or disaggregation of nanoparticles[21,32,40,113] which have demonstrated the dramatic signal changes that are possible. Our work highlights the gains in sensitivity that can be made using such systems and presents a platform for developing a range of high relaxivity contrast agents for detecting small molecules. A broader range of *in vivo* studies could be pursued using the nanoparticle iteration of the BM3h sensors, in part to demonstrate the broader possible utility of such systems. *In vivo* neuroimaging with nanoparticle sensors has been shown to be possible in the context of calcium imagine.[143]

Our nanoparticle sensor, and others like it, faces some limitations to be addressed in future work. One issue is the slow reaggregation kinetics of the multicomponent system. Rodriguez *et al.* from our group have found that using two components of different sizes can accelerate aggregation kinetics compared to a system using two nanoparticle species of the same size.[113] Reaggregation of nanoparticles may also be slow due to dilution of the sensor as it is taken up by cells or diffuses from the injection site. These effects could be addressed by encapsulating the sensor components together in a membrane prior to delivery, or loosely tethering the nanoparticles together to limit the distance that the components can travel apart. For encapsulation, liposomes or red blood cell (RBC) ghosts could be used, though pores would need

to be introduced to allow the analyte to interact with the nanoparticles.[144–147] Encapsulation of the sensor could also slow or prevent the uptake of the nanoparticles by cells. A fundamental challenge of all contrast agents for neuroimaging is the difficulty of delivering the probes non-invasively to the brain.[82] For non-invasive delivery of nanoparticle-based sensors, the most suitable methods in development are hyperosmotic shock or ultrasound.

In this work I also investigated the feasibility of using semi-rational protein design to engineer a high relaxivity metalloprotein by improving gadolinium binding using PAH as the protein scaffold. The gadolinium binding of the protein was improved by two orders of magnitude to obtain submicromolar $K_d$ with modest dopamine-modulated relaxivity changes of about 15% observed. Incorporating computational protein engineering methods could aid in designing a tighter gadolinium binding site to reduce the toxicity of the agent. However, experimental screening methods are likely still required to examine relaxivity due to the current limitations of computational methods.[138] A semi-rational approach could also be pursued to improve the ligand responsiveness of the PAH mutants.

Proteins and peptides that bind one lanthanide are likely able to bind others, which suggests that gadolinium-binding PAH could be adapted as a CEST agent by swapping gadolinium for europium. Terbium could also be incorporated for the development of a dual modality imaging agent that can be detected by both MRI and fluorescence. CEST agents generally need to be applied at higher concentrations compared to other bioengineered contrast agents for ${}^1$H MRI[148] but may be useful in situations requiring differential detection of the probe.

# 5 References

(1) Gadian, D. G. (1995) NMR and its applications to living systems. Oxford University Press.

(2) Buxton, R. B. (2002) Introduction to Functional Magnetic Resonance Imaging: Principles and Techniques. Cambridge University Press.

(3) Jasanoff, A. (2007) MRI contrast agents for functional molecular imaging of brain activity. *Curr. Opin. Neurobiol. 17*, 593–600.

(4) Lauffer, R. B. (1987) Paramagnetic metal complexes as water proton relaxation agents for NMR imaging: theory and design. *Chem. Rev. 87*, 901–927.

(5) Toth, E., Helm, L., and Merbach, A. E. (2002) Relaxivity of MRI contrast agents. *Top. Curr. Chem. 221*, 61–101.

(6) Schwert, D. D., Davies, J. A., and Richardson, N. (2002) Non-gadolinium-based MRI contrast agents. *Top. Curr. Chem. 221*, 165–199.

(7) Ward, K. M., Aletras, A. H., and Balaban, R. S. (2000) A New Class of Contrast Agents for MRI Based on Proton Chemical Exchange Dependent Saturation Transfer (CEST). *J. Magn. Reson. 143*, 79–87.

(8) Mildvan, A. S. (1974) Mechanism of Enzyme Action. *Annu. Rev. Biochem. 43*, 357–399.

(9) Burton, D. R., Forsen, S., Karlstrom, G., and Dwek, R. A. (1979) Proton relaxation enhancement (PRE) in biochemistry: A critical survey. *Prog. Nucl. Magn. Reson. Spectrosc. 13*, 1–45.

(10) Westmeyer, G. G., and Jasanoff, A. (2007) Genetically controlled MRI contrast mechanisms and their prospects in systems neuroscience research. *Magn. Reson. Imaging 25*, 1004–1010.

(11) Shimomura, O., Johnson, F. H., and Saiga, Y. (1962) Extraction, Purification and Properties of Aequorin, a Bioluminescent Protein from the Luminous Hydromedusan, Aequorea. *J. Cell. Comp. Physiol. 59*, 223–239.

(12) Giepmans, B. N. G., Adams, S. R., Ellisman, M. H., and Tsien, R. Y. (2006) The Fluorescent Toolbox for Assessing Protein Location and Function. *Science 312*, 217–224.

(13) Pauling, L., and Coryell, C. D. (1936) The magnetic properties and structure of hemoglobin, oxyhemoglobin and carbonmonoxyhemoglobin. *Proc. Natl. Acad. Sci. U. S. A. 22*, 210–216.

(14) Ogawa, S., Lee, T.-M., Kay, A. R., and Tank, D. W. (1990) Brain magnetic resonance imaging with contrast dependent on blood oxygenation. *Proc. Natl. Acad. Sci. U. S. A. 87*, 9868–9872.

(15) Ogawa, S., Tank, D. W., Menon, R., Ellerman, J. M., Kim, S.-G., Merkle, H., and Ugurbil, K. (1992) Intrinsic signal changes accompanying sensory stimulation: functional brain mapping with magnetic resonance imaging. *Proc. Natl. Acad. Sci. U. S. A. 89*, 5951–5955.

(16) Kwong, K. K., Belliveau, J. W., Chesler, D. A., Goldberg, I. E., Weisskoff, R. M., Poncelet, B. P., Kennedy, D. N., Hoppel, B. E., Cohen, M. S., Turner, R., Cheng, H.-M., Brady, T. J., and Rosen, B. R. (1992) Dynamic magnetic resonance imaging of human brain activity during primary sensory stimulation. *Proc. Natl. Acad. Sci. U. S. A. 89*, 5675–5679.

(17) Sun, P. Z., Schoening, Z. B., and Jasanoff, A. (2003) In vivo oxygen detection using exogenous hemoglobin as a contrast agent in magnetic resonance microscopy. *Magn. Reson. Med. 49*, 609–614.

(18) Shapiro, M. G., Westmeyer, G. G., Romero, P. A., Szablowski, J. O., Küster, B., Shah, A., Otey, C. R., Langer, R., Arnold, F. H., and Jasanoff, A. (2010) Directed evolution of a magnetic resonance imaging contrast agent for noninvasive imaging of dopamine. *Nat. Biotechnol. 28*, 264–270.

(19) Brustad, E. M., and Arnold, F. H. (2011) Optimizing non-natural protein function with directed evolution. *Curr. Opin. Chem. Biol. 15*, 201–210.

(20) Lelyveld, V. S., Brustad, E., Arnold, F. H., and Jasanoff, A. (2011) Metal-Substituted Protein MRI Contrast Agents Engineered for Enhanced Relaxivity and Ligand Sensitivity. *J. Am. Chem. Soc. 133*, 649–651.

(21) Atanasijevic, T., Shusteff, M., Fam, P., and Jasanoff, A. (2006) Calcium-sensitive MRI contrast agents based on superparamagnetic iron oxide nanoparticles and calmodulin. *Proc. Natl. Acad. Sci. U. S. A. 103*, 14707–14712.

(22) Smith, G. A., Hesketh, R. T., Metcalfe, J. C., Feeney, J., and Morris, P. G. (1983) Intracellular calcium measurements by 19F NMR of fluorine-labeled chelators. *Proc. Natl. Acad. Sci. U. S. A. 80*, 7178–7182.

(23) Li, W., Fraser, S. E., and Meade, T. J. (1999) A Calcium-Sensitive Magnetic Resonance Imaging Contrast Agent. *J. Am. Chem. Soc. 121*, 1413–1414.

(24) Green, D. F., Dennis, A. T., Fam, P. S., Tidor, B., and Jasanoff, A. (2006) Rational Design of New Binding Specificity by Simultaneous Mutagenesis of Calmodulin and a Target Peptide. *Biochemistry 45*, 12547–12559.

(25) Gilad, A. A., McMahon, M. T., Walczak, P., Winnard, P. T., Raman, V., van Laarhoven, H. W. M., Skoglund, C. M., Bulte, J. W. M., and van Zijl, P. C. M. (2007) Artificial reporter gene providing MRI contrast based on proton exchange. *Nat. Biotechnol. 25*, 217–219.

(26) McMahon, M. T., Gilad, A. A., DeLiso, M. A., Cromer Berman, S. M., Bulte, J. W. M., and van Zijl, P. C. M. (2008) New "multicolor" polypeptide diamagnetic chemical exchange saturation transfer (DIACEST) contrast agents for MRI. *Magn. Reson. Med. 60*, 803–812.

(27) Prescher, J. A., and Contag, C. H. (2010) Guided by the light: visualizing biomolecular processes in living animals with bioluminescence. *Curr. Opin. Chem. Biol. 14*, 80–89.

(28) Louie, A. Y., Hüber, M. M., Ahrens, E. T., Rothbächer, U., Moats, R., Jacobs, R. E., Fraser, S. E., and Meade, T. J. (2000) In vivo visualization of gene expression using magnetic resonance imaging. *Nat. Biotechnol. 18*, 321–325.

(29) Himmelreich, U., Aime, S., Hieronymus, T., Justicia, C., Uggeri, F., Zenke, M., and Hoehn, M. (2006) A responsive MRI contrast agent to monitor functional cell status. *NeuroImage 32*, 1142–1149.

(30) Mizukami, S., Takikawa, R., Sugihara, F., Hori, Y., Tochio, H., Wälchli, M., Shirakawa, M., and Kikuchi, K. (2008) Paramagnetic Relaxation-Based 19F MRI Probe To Detect Protease Activity. *J. Am. Chem. Soc. 130*, 794–795.

(31) Rodriguez, E., Nilges, M., Weissleder, R., and Chen, J. W. (2010) Activatable Magnetic Resonance Imaging Agents for Myeloperoxidase Sensing: Mechanism of Activation, Stability, and Toxicity. *J. Am. Chem. Soc. 132*, 168–177.

(32) Perez, J. M., Simeone, F. J., Tsourkas, A., Josephson, L., and Weissleder, R. (2004) Peroxidase Substrate Nanosensors for MR Imaging. *Nano Lett. 4*, 119–122.

(33) Weissleder, R., Simonova, M., Bogdanova, A., Bredow, S., Enochs, W. S., and Bogdanov, A. (1997) MR imaging and scintigraphy of gene expression through melanin induction. *Radiology 204*, 425–429.

(34) Haacke, E. M., Cheng, N. Y. C., House, M. J., Liu, Q., Neelavalli, J., Ogg, R. J., Khan, A., Ayaz, M., Kirsch, W., and Obenaus, A. (2005) Imaging iron stores in the brain using magnetic resonance imaging. *Magn. Reson. Imaging 23*, 1–25.

(35) Wang, Y.-X. J., Hussain, S. M., and Krestin, G. P. (2001) Superparamagnetic iron oxide contrast agents: physicochemical characteristics and applications in MR imaging. *Eur. Radiol.* *11*, 2319–2331.

(36) Weissleder, R., Moore, A., Mahmood, U., Bhorade, R., Benveniste, H., Chiocca, E. A., and Basilion, J. P. (2000) In vivo magnetic resonance imaging of transgene expression. *Nat. Med. N. Y.* *6*, 351–354.

(37) Olson, E. S., Jiang, T., Aguilera, T. A., Nguyen, Q. T., Ellies, L. G., Scadeng, M., and Tsien, R. Y. (2010) Activatable cell penetrating peptides linked to nanoparticles as dual probes for in vivo fluorescence and MR imaging of proteases. *Proc. Natl. Acad. Sci. U. S. A.* *107*, 4311–4316.

(38) Egeblad, M., and Werb, Z. (2002) New functions for the matrix metalloproteinases in cancer progression. *Nat. Rev. Cancer 2*, 161–174.

(39) Jiang, T., Olson, E. S., Nguyen, Q. T., Roy, M., Jennings, P. A., and Tsien, R. Y. (2004) Tumor imaging by means of proteolytic activation of cell-penetrating peptides. *Proc. Natl. Acad. Sci. U. S. A.* *101*, 17867–17872.

(40) Westmeyer, G. G., Durocher, Y., and Jasanoff, A. (2010) A Secreted Enzyme Reporter System for MRI. *Angew. Chem. Int. Ed.* *49*, 3909–3911.

(41) Hanaoka, K., Kikuchi, K., Terai, T., Komatsu, T., and Nagano, T. (2008) A Gd3+-based magnetic resonance imaging contrast agent sensitive to β-galactosidase activity utilizing a receptor-induced magnetization enhancement (RIME) phenomenon. *Chem. - Eur. J.* *14*, 987–995.

(42) Cui, W., Liu, L., Kodibagkar, V. D., and Mason, R. P. (2010) S-Gal, a novel 1H MRI reporter for β-galactosidase. *Magn. Reson. Med.* *64*, 65–71.

(43) Arena, F., Singh, J. B., Gianolio, E., Stefania, R., and Aime, S. (2011) β-Gal Gene Expression MRI Reporter in Melanoma Tumor Cells. Design, Synthesis, and in Vitro and in Vivo Testing of a Gd(III) Containing Probe Forming a High Relaxivity, Melanin-Like Structure upon β-Gal Enzymatic Activation. *Bioconjug. Chem.* *22*, 2625–2635.

(44) Keliris, A., Ziegler, T., Mishra, R., Pohmann, R., Sauer, M. G., Ugurbil, K., and Engelmann, J. (2011) Synthesis and characterization of a cell-permeable bimodal contrast agent targeting β-galactosidase. *Bioorg. Med. Chem.* *19*, 2529–2540.

(45) Yigit, M. V., Mazumdar, D., and Lu, Y. (2008) MRI Detection of Thrombin with Aptamer Functionalized Superparamagnetic Iron Oxide Nanoparticles. *Bioconjug. Chem. 19*, 412–417.

(46) Granot, D., and Shapiro, E. M. (2011) Release activation of iron oxide nanoparticles: (REACTION) A novel environmentally sensitive MRI paradigm. *Magn. Reson. Med. 65*, 1253–1259.

(47) Sipkins, D. A., Cheresh, D. A., Kazemi, M. R., Nevin, L. M., Bednarski, M. D., and Li, K. C. P. (1998) Detection of tumor angiogenesis in vivo by αvβ3-targeted magnetic resonance imaging. *Nat. Med. N. Y. 4*, 623–626.

(48) Tsourkas, A., Shinde-Patil, V. R., Kelly, K. A., Patel, P., Wolley, A., Allport, J. R., and Weissleder, R. (2005) In Vivo imaging of activated endothelium using an anti-VCAM-1 magnetooptical probe. *Bioconjug. Chem. 16*, 576–581.

(49) McAteer, M. A., Sibson, N. R., von zur Muhlen, C., Schneider, J. E., Lowe, A. S., Warrick, N., Channon, K. M., Anthony, D. C., and Choudhury, R. P. (2007) In vivo magnetic resonance imaging of acute brain inflammation using microparticles of iron oxide. *Nat. Med. N. Y. 13*, 1253–1258.

(50) Caravan, P., Das, B., Dumas, S., Epstein, F. H., Helm, P. A., Jacques, V., Koerner, S., Kolodziej, A., Shen, L., Sun, W.-C., and Zhang, Z. (2007) Collagen-targeted MRI contrast agent for molecular imaging of fibrosis. *Angew. Chem. Int. Ed. 46*, 8171–8173.

(51) Nair, S. A., Kolodziej, A. F., Bhole, G., Greenfield, M. T., McMurry, T. J., and Caravan, P. (2008) Monovalent and bivalent fibrin-specific MRI contrast agents for detection of thrombus. *Angew. Chem. Int. Ed. 47*, 4918–4921.

(52) Overoye-Chan, K., Koerner, S., Looby, R. J., Kolodziej, A. F., Zech, S. G., Deng, Q., Chasse, J. M., McMurry, T. J., and Caravan, P. (2008) EP-2104R: A Fibrin-Specific Gadolinium-Based MRI Contrast Agent for Detection of Thrombus. *J. Am. Chem. Soc. 130*, 6025–6039.

(53) Kolodziej, A. F., Nair, S. A., Graham, P., McMurry, T. J., Ladner, R. C., Wescott, C., Sexton, D. J., and Caravan, P. (2012) Fibrin Specific Peptides Derived by Phage Display: Characterization of Peptides and Conjugates for Imaging. *Bioconjug. Chem. 23*, 548–556.

(54) Enochs, W. S., Schaffer, B., Bhide, P. G., Nossiff, N., Papisov, M., Bogdanov, A. J., Brady, T. J., and Weissleder, R. (1993) MR imaging of slow axonal transport in vivo. *Exp. Neurol. 123*, 235–242.

(55) Petropoulos, A. E., Schaffer, B. K., Cheney, M. L., Enochs, S., Zimmer, C., and Weissleder, R. (1995) MR imaging of neuronal transport in the guinea pig facial nerve: initial findings. *Acta Otolaryngol 115*, 512–516.

(56) van Everdingen, K. J., Enochs, W. S., Bhide, P. G., Nossiff, N., Papisov, M., Bogdanov, A. J., Brady, T. J., and Weissleder, R. (1994) Determinants of in vivo MR imaging of slow axonal transport. *Radiology 193*, 485–491.

(57) Wu, C. W.-H., Vasalatiy, O., Liu, N., Wu, H., Cheal, S., Chen, D.-Y., Koretsky, A. P., Griffiths, G. L., Tootell, R. B. H., and Ungerleider, L. G. (2011) Development of a MR-Visible Compound for Tracing Neuroanatomical Connections In Vivo. *Neuron 70*, 229–243.

(58) Vercelli, A., Repici, M., Garbossa, D., and Grimaldi, A. (2000) Recent techniques for tracing pathways in the central nervous system of developing and adult mammals. *Brain Res. Bull. 51*, 11–28.

(59) van Kasteren, S. I., Campbell, S. J., Serres, S., Anthony, D. C., Sibson, N. R., and Davis, B. G. (2009) Glyconanoparticles allow pre-symptomatic in vivo imaging of brain disease. *Proc. Natl. Acad. Sci. U. S. A. 106*, 18–23.

(60) Ellington, A. D., and Szostak, J. W. (1990) In vitro selection of RNA molecules that bind specific ligands. *Nature 346*, 818–22.

(61) Stoltenburg, R., Reinemann, C., and Strehlitz, B. (2007) SELEX-A (r)evolutionary method to generate high-affinity nucleic acid ligands. *Biomol. Eng. 24*, 381–403.

(62) Liu, C. H., Huang, S., Cui, J., Kim, Y. R., Farrar, C. T., Moskowitz, M. A., Rosen, B. R., and Liu, P. K. (2007) MR contrast probes that trace gene transcripts for cerebral ischemia in live animals. *FASEB J.* 3004–3015.

(63) Liu, C. H., Ren, J. Q., Yang, J., Liu, C., Mandeville, J. B., Rosen, B. R., Bhide, P. G., Yanagawa, Y., and Liu, P. K. (2009) DNA-based MRI probes for specific detection of chronic exposure to amphetamine in living brains. *J. Neurosci. 29*, 10663–10670.

(64) Liu, C. H., Ren, J. Q., You, Z., Yang, J., Liu, C.-M., Uppal, R., and Liu, P. K. (2012) Noninvasive detection of neural progenitor cells in living brains by MRI. *FASEB J. 26*, 1652–1662.

(65) Liu, C. H., You, Z., Ren, J., Kim, Y. R., Eikermann-Haerter, K., and Liu, P. K. (2008) Noninvasive delivery of gene targeting probes to live brains for transcription MRI. *FASEB J. 22*, 1193–1203.

(66) Lelyveld, V. S., Atanasijevic, T., and Jasanoff, A. (2010) Challenges for molecular neuroimaging with MRI. *Int. J. Imaging Syst. Technol. 20*, 71–79.

(67) Gilad, A. A., Winnard, P. T., Jr., van Zijl, P. C. M., and Bulte, J. W. M. (2007) Developing MR reporter genes: promises and pitfalls. *NMR Biomed. 20*, 275–290.

(68) Genove, G., DeMarco, U., Xu, H., Goins, W. F., and Ahrens, E. T. (2005) A new transgene reporter for in vivo magnetic resonance imaging. *Nat. Med. N. Y. 11*, 450–454.

(69) Cohen, B., Dafni, H., Meir, G., Harmelin, A., and Neeman, M. (2005) Ferritin as an endogenous MRI reporter for noninvasive imaging of gene expression in C6 glioma tumors. *Neoplasia 7*, 109–117.

(70) Cohen, B., Ziv, K., Plaks, V., Israely, T., Kalchenko, V., Harmelin, A., Benjamin, L. E., and Neeman, M. (2007) MRI detection of transcriptional regulation of gene expression in transgenic mice. *Nat. Med. N. Y. 13*, 498–503.

(71) Meldrum, F. C., Heywood, B. R., and Mann, S. (1992) Magnetoferritin: in vitro synthesis of a novel magnetic protein. *Science 257*, 522–523.

(72) Deans, A. E., Wadghiri, Y. Z., Bernas, L. M., Yu, X., Rutt, B. K., and Turnbull, D. H. (2006) Cellular MRI contrast via coexpression of transferrin receptor and ferritin. *Magn. Reson. Med. 56*, 51–59.

(73) Matsumoto, Y., Chen, R., Anikeeva, P., and Jasanoff, A. (2015) Engineering intracellular biomineralization and biosensing by a magnetic protein. *Nat. Commun. 6*, 8721-8730.

(74) Zurkiya, O., Chan, A. W. S., and Hu, X. (2008) MagA is sufficient for producing magnetic nanoparticles in mammalian cells, making it an MRI reporter. *Magn. Reson. Med. 59*, 1225–1231.

(75) Goldhawk, D. E., Lemaire, C., McCreary, C. R., McGirr, R., Dhanvantari, S., Thompson, R. T., Figueredo, R., Koropatnick, J., Foster, P., and Prato, F. S. (2009) Magnetic resonance imaging of cells overexpressing MagA, an endogenous contrast agent for live cell imaging. *Mol. Imaging 8*, 129–139.

(76) van Zijl, P. C. M., Zhou, J., Mori, N., Payen, J.-F., Wilson, D., and Mori, S. (2003) Mechanism of magnetization transfer during on-resonance water saturation. A new approach to detect mobile proteins, peptides, and lipids. *Magn. Reson. Med. 49*, 440–449.

(77) Zhou, J., Payen, J.-F., Wilson, D. A., Traystman, R. J., and van Zijl, P. C. M. (2003) Using the amide proton signals of intracellular proteins and peptides to detect pH effects in MRI. *Nat. Med. N. Y. 9*, 1085–1090.

(78) Pérez-Torres, C. J., Massaad, C. A., Hilsenbeck, S. G., Serrano, F., and Pautler, R. G. (2010) In vitro and in vivo magnetic resonance imaging (MRI) detection of GFP through magnetization transfer contrast (MTC). *NeuroImage 50*, 375–382.

(79) Gossuin, Y., Muller, R. N., Gillis, P., and Bartel, L. (2005) Relaxivities of human liver and spleen ferritin. *Magn. Reson. Imaging 23*, 1001–1004.

(80) Jung, C. W., and Jacobs, P. (1995) Physical and chemical properties of superparamagnetic iron oxide MR contrast agents: ferumoxides, ferumoxtran, ferumoxsil. *Magn. Reson. Imaging 13*, 661–674.

(81) Zhang, S., Merritt, M., Woessner, D. E., Lenkinski, R. E., and Sherry, A. D. (2003) PARACEST Agents: Modulating MRI Contrast via Water Proton Exchange. *Acc. Chem. Res. 36*, 783–790.

(82) Vykhodtseva, N., McDannold, N., and Hynynen, K. (2008) Progress and problems in the application of focused ultrasound for blood-brain barrier disruption. *Ultrasonics 48*, 279–296.

(83) Roman-Goldstein, S. M., Barnett, P. A., McCormick, C. I., Szumowski, J., Shannon, E. M., Ramsey, F. L., Mass, M., and Neuwelt, E. A. (1994) Effects of Gd-DTPA after osmotic BBB disruption in a rodent model: toxicity and MR findings. *J. Comput. Assist. Tomogr. 18*, 731–736.

(84) Norman, A. B., Bertram, K. J., Thomas, S. R., Pratt, R. G., Samaratunga, R. C., and Sanberg, P. R. (1991) Magnetic resonance imaging of rat brain following in vivo disruption of the cerebral vasculature. *Brain Res. Bull. 26*, 593–597.

(85) Hynynen, K., McDannold, N., Sheikov, N. A., Jolesz, F. A., and Vykhodtseva, N. (2005) Local and reversible blood–brain barrier disruption by noninvasive focused ultrasound at frequencies suitable for trans-skull sonications. *NeuroImage 24*, 12–20.

(86) Neuwelt, E. A., Weissleder, R., Nilaver, G., Kroll, R. A., Roman-Goldstein, S., Szumowski, J., Pagel, M. A., Jones, R. S., Remsen, L. G., and McCormick, C. I. (1994) Delivery of virus-sized iron oxide particles to rodent CNS neurons. *Neurosurgery 34*, 777–784.

(87) Muldoon, L. L., Sàndor, M., Pinkston, K. E., and Neuwelt, E. A. (2005) Imaging, distribution, and toxicity of superparamagnetic iron oxide magnetic resonance nanoparticles in the rat brain and intracerebral tumor. *Neurosurgery 57*, 785–796.

(88) Hynynen, K., McDannold, N., Vykhodtseva, N., Raymond, S., Weissleder, R., Jolesz, F. A., and Sheikov, N. (2006) Focal disruption of the blood-brain barrier due to 260-kHz ultrasound bursts: a method for molecular imaging and targeted drug delivery. *J. Neurosurg. 105*, 445–454.

(89) Neuwelt, E. A., and Rapoport, S. I. (1984) Modification of the blood-brain barrier in the chemotherapy of malignant brain tumors. *Fed. Proc. 43*, 214–219.

(90) McDannold, N., Arvanitis, C. D., Vykhodtseva, N., and Livingstone, M. S. (2012) Temporary Disruption of the Blood-Brain Barrier by Use of Ultrasound and Microbubbles: Safety and Efficacy Evaluation in Rhesus Macaques. *Cancer Res. 72*, 3652–3663.

(91) Choi, J. J., Wang, S., Tung, Y.-S., Morrison III, B., and Konofagou, E. E. (2010) Molecules of Various Pharmacologically-Relevant Sizes Can Cross the Ultrasound-Induced Blood-Brain Barrier Opening in vivo. *Ultrasound Med. Biol. 36*, 58–67.

(92) Caravan, P., Cloutier, N. J., Greenfield, M. T., McDermid, S. A., Dunham, S. U., Bulte, J. W. M., Amedio, J. C., Jr., Looby, R. J., Supkowski, R. M., Horrocks, W. D., Jr., McMurry, T. J., and Lauffer, R. B. (2002) The Interaction of MS-325 with Human Serum Albumin and Its Effect on Proton Relaxation Rates. *J. Am. Chem. Soc. 124*, 3152–3162.

(93) Caravan, P., Parigi, G., Chasse, J. M., Cloutier, N. J., Ellison, J. J., Lauffer, R. B., Luchinat, C., McDermid, S. A., Spiller, M., and McMurry, T. J. (2007) Albumin Binding, Relaxivity, and Water Exchange Kinetics of the Diastereoisomers of MS-325, a Gadolinium(III)-Based Magnetic Resonance Angiography Contrast Agent. *Inorg. Chem. 46*, 6632–6639.

(94) Caravan, P. (2009) Protein-Targeted Gadolinium-Based Magnetic Resonance Imaging (MRI) Contrast Agents: Design and Mechanism of Action. *Acc. Chem. Res. 42*, 851–862.

(95) Zech, S. G., Eldredge, H. B., Lowe, M. P., and Caravan, P. (2007) Protein Binding to Lanthanide(III) Complexes Can Reduce the Water Exchange Rate at the Lanthanide. *Inorg. Chem. 46*, 3576–3584.

(96) Faivre, D., and Schueler, D. (2008) Magnetotactic Bacteria and Magnetosomes. *Chem. Rev. 108*, 4875–4898.

(97) Walcott, C., Gould, J. L., and Kirschvink, J. L. (1979) Pigeons have magnets. *Science 205*, 1027–1029.

(98) Kuterbach, D. A., Walcott, B., Reeder, R. J., and Frankel, R. B. (1982) Iron-containing cells in the honey bee (Apis mellifera). *Science. 218*, 695–697.

(99) Beason, R. C., and Nichols, J. E. (1984) Magnetic orientation and magnetically sensitive material in a transequatorial migratory bird. *Nature 309*, 151–153.

(100) Zoeger, J., Dunn, J. R., and Fuller, M. (1981) Magnetic material in the head of the common Pacific dolphin. *Science 213*, 892–894.

(101) Pardridge, W. M. (2008) Re-Engineering Biopharmaceuticals for Delivery to Brain with Molecular Trojan Horses. *Bioconjug. Chem. 19*, 1327–1338.

(102) Wang, T., Town, T., Alexopoulou, L., Anderson, J. F., Fikrig, E., and Flavell, R. A. (2004) Toll-like receptor 3 mediates West Nile virus entry into the brain causing lethal encephalitis. *Nat. Med. N. Y. 10*, 1366–1373.

(103) Koenig, S., Gendelman, H. E., Orenstein, J. M., Dal, C. M. C., Pezeshkpour, G. H., Yungbluth, M., Janotta, F., Aksamit, A., Martin, M. A., and Fauci, A. S. (1986) Detection of AIDS virus in macrophages in brain tissue from AIDS patients with encephalopathy. *Science 233*, 1089–1093.

(104) Fink, D. J., and Glorioso, J. C. (1997) Engineering herpes simplex virus vectors for gene transfer to neurons. *Nat. Med. N. Y. 3*, 357–359.

(105) Deverman, B. E., Pravdo, P. L., Simpson, B. P., Kumar, S. R., Chan, K. Y., Banerjee, A., Wu, W.-L., Yang, B., Huber, N., Pasca, S. P., and Gradinaru, V. (2016) Cre-dependent selection yields AAV variants for widespread gene transfer to the adult brain. *Nat. Biotechnol. 34*, 204–209.

(106) Logothetis, N. K. (2008) What we can do and what we cannot do with fMRI. *Nature 453*, 869–878.

(107) Hsieh, V., and Jasanoff, A. (2012) Bioengineered Probes for Molecular Magnetic Resonance Imaging in the Nervous System. *ACS Chem. Neurosci. 3*, 593–602.

(108) Brustad, E. M., Lelyveld, V. S., Snow, C. D., Crook, N., Jung, S. T., Martinez, F. M., Scholl, T. J., Jasanoff, A., and Arnold, F. H. (2012) Structure-Guided Directed Evolution of Highly Selective P450-Based Magnetic Resonance Imaging Sensors for Dopamine and Serotonin. *J. Mol. Biol. 422*, 245–262.

(109) Lee, T., Cai, L. X., Lelyveld, V. S., Hai, A., and Jasanoff, A. (2014) Molecular-Level Functional Magnetic Resonance Imaging of Dopaminergic Signaling. *Science 344*, 533–535.

(110) Hai, A., Cai, L. X., Lee, T., Lelyveld, V. S., and Jasanoff, A. (2015, December 22) Molecular fMRI of serotonin transport. Submitted manuscript.

(111) Sosnovik, D. E., and Weissleder, R. (2007) Emerging concepts in molecular MRI. *Curr. Opin. Biotechnol. 18*, 4–10.

(112) Matsumoto, Y., and Jasanoff, A. (2008) T2 relaxation induced by clusters of superparamagnetic nanoparticles: Monte Carlo simulations. *Magn. Reson. Imaging 26*, 994–998.

(113) Rodriguez, E., Lelyveld, V. S., Atanasijevic, T., Okada, S., and Jasanoff, A. (2014) Magnetic nanosensors optimized for rapid and reversible self-assembly. *Chem. Commun. 50*, 3595-3598.

(114) Miller, D. D., Hamada, A., Clark, M. T., Adejare, A., Patil, P. N., Shams, G., Romstedt, K. J., Kim, S. U., and Intrasuksri, U. (1990) Synthesis and alpha-2-adrenoceptor effects of substituted catecholimidazoline and catecholimidazole analogs in human platelets. *J. Med. Chem. 33*, 1138–1144.

(115) Yeo, W.-S., Min, D.-H., Hsieh, R. W., Greene, G. L., and Mrksich, M. (2005) Label-Free Detection of Protein–Protein Interactions on Biochips. *Angew. Chem. Int. Ed. 44*, 5480–5483.

(116) Hanauer, M., Pierrat, S., Zins, I., Lotz, A., and Sönnichsen, C. (2007) Separation of Nanoparticles by Gel Electrophoresis According to Size and Shape. *Nano Lett. 7*, 2881–2885.

(117) Omura, T., and Sato, R. (1964) The Carbon Monoxide-binding Pigment of Liver Microsomes. *J. Biol. Chem. 239*, 2370–2378.

(118) Aime, S., Barge, A., Botta, M., and Terreno, E. (2002) Interactions of lanthanides and their complexes with proteins. Conclusions regarding magnetic resonance imaging. *Met. Ions Biol. Syst. 40*, 643–682.

(119) Burroughs, S. E., Horrocks, W. D., Ren, H., and Klee, C. B. (1994) Characterization of the Lanthanide Ion-Binding Properties of Calcineurin-B Using Laser-Induced Luminescence Spectroscopy. *Biochemistry 33*, 10428–10436.

(120) Pidcock, E., and Moore, G. R. (2001) Structural characteristics of protein binding sites for calcium and lanthanide ions. *J. Biol. Inorg. Chem. 6*, 479–489.

(121) Barbieri, R., Bertini, I., Cavallaro, G., Lee, Y.-M., Luchinat, C., and Rosato, A. (2002) Paramagnetically Induced Residual Dipolar Couplings for Solution Structure Determination of Lanthanide Binding Proteins. *J. Am. Chem. Soc. 124*, 5581–5587.

(122) Rodriguez-Castañeda, F., Haberz, P., Leonov, A., and Griesinger, C. (2006) Paramagnetic tagging of diamagnetic proteins for solution NMR. *Magn. Reson. Chem. 44*, S10–S16.

(123) Franz, K. J., Nitz, M., and Imperiali, B. (2003) Lanthanide-Binding Tags as Versatile Protein Coexpression Probes. *ChemBioChem 4*, 265–271.

(124) Reynolds, A. M., Sculimbrene, B. R., and Imperiali, B. (2008) Lanthanide-Binding Tags with Unnatural Amino Acids: Sensitizing Tb3+ and Eu3+ Luminescence at Longer Wavelengths. *Bioconjug. Chem. 19*, 588–591.

(125) Allen, K. N., and Imperiali, B. (2010) Lanthanide-tagged proteins—an illuminating partnership. *Curr. Opin. Chem. Biol. 14*, 247–254.

(126) Berwick, M. R., Lewis, D. J., Jones, A. W., Parslow, R. A., Dafforn, T. R., Cooper, H. J., Wilkie, J., Pikramenou, Z., Britton, M. M., and Peacock, A. F. A. (2014) De Novo Design of Ln(III) Coiled Coils for Imaging Applications. *J. Am. Chem. Soc. 136*, 1166–1169.

(127) Berwick, M. R., Slope, L. N., Smith, C. F., King, S. M., Newton, S. L., Gillis, R. B., Adams, G. G., Rowe, A. J., Harding, S. E., Britton, M. M., and Peacock, A. F. A. (2016) Location dependent coordination chemistry and MRI relaxivity, in de novo designed lanthanide coiled coils. *Chem. Sci. 7*, 2207–2216.

(128) Jervis, G. A. (1947) Studies on phenylpyruvic oligophrenia The position of the metabolic error. *J. Biol. Chem. 169*, 651–656.

(129) Fusetti, F., Erlandsen, H., Flatmark, T., and Stevens, R. C. (1998) Structure of Tetrameric Human Phenylalanine Hydroxylase and Its Implications for Phenylketonuria. *J. Biol. Chem. 273*, 16962–16967.

(130) Miller, M. R., and Shiman, R. (1976) Reversible inactivation of phenylalanine hydroxylase by catecholamines in cultured hepatoma cells. *J. Biol. Chem. 251*, 3671–3676.

(131) Martínez, A., Haavik, J., and Flatmark, T. (1990) Cooperative homotropic interaction of l-noradrenaline with the catalytic site of phenylalanine 4-monooxygenase. *Eur. J. Biochem. 193*, 211–219.

(132) Martínez, A., Andersson, K. K., Haavik, J., and Flatmark, T. (1991) EPR and 1H-NMR spectroscopic studies on the paramagnetic iron at the active site of phenylalanine hydroxylase and its interaction with substrates and inhibitors. *Eur. J. Biochem. 198*, 675–682.

(133) Hagedoorn, P.-L., Schmidt, P. P., Andersson, K. K., Hagen, W. R., Flatmark, T., and Martinez, A. (2001) The Effect of Substrate, Dihydrobiopterin, and Dopamine on the EPR Spectroscopic Properties and the Midpoint Potential of the Catalytic Iron in Recombinant Human Phenylalanine Hydroxylase. *J. Biol. Chem. 276*, 22850–22856.

(134) Erlandsen, H., Flatmark, T., Stevens, R. C., and Hough, E. (1998) Crystallographic Analysis of the Human Phenylalanine Hydroxylase Catalytic Domain with Bound Catechol Inhibitors at 2.0 Å Resolution. *Biochemistry 37*, 15638–15646.

(135) Erlandsen, H., Kim, J. Y., Patch, M. G., Han, A., Volner, A., Abu-Omar, M. M., and Stevens, R. C. (2002) Structural Comparison of Bacterial and Human Iron-dependent Phenylalanine Hydroxylases: Similar Fold, Different Stability and Reaction Rates. *J. Mol. Biol. 320*, 645–661.

(136) Que, L. (2000) One motif-many different reactions. *Nat. Struct. Biol. 7*, 182–183.

(137) Sherry, A. D., Caravan, P., and Lenkinski, R. E. (2009) Primer on gadolinium chemistry. *J. Magn. Reson. Imaging 30*, 1240–1248.

(138) Lippow, S. M., and Tidor, B. (2007) Progress in computational protein design. *Curr. Opin. Biotechnol. 18*, 305–311.

(139) Lutz, S. (2010) Beyond directed evolution - semi-rational protein engineering and design. *Curr. Opin. Biotechnol. 21*, 734–743.

(140) Snyder, E. E., Buoscio, B. W., and Falke, J. J. (1990) Calcium (II) site specificity: effect of size and charge on metal ion binding to an EF-hand-like site. *Biochemistry (Mosc.) 29*, 3937–3943.

(141) Rohrer, M., Bauer, H., Mintorovitch, J., Requardt, M., and Weinmann, H.-J. (2005) Comparison of magnetic properties of MRI contrast media solutions at different magnetic field strengths. *Invest. Radiol. 40*, 715–724.

(142) Garris, P. A., Ciolkowski, E. L., Pastore, P., and Wightman, R. M. (1994) Efflux of dopamine from the synaptic cleft in the nucleus accumbens of the rat brain. *J. Neurosci. 14*, 6084–6093.

(143) Okada, S., Bartelle, B. B., and Jasanoff, A. (In preparation).

(144) Steck, T. L., and Kant, J. A. (1974) Preparation of impermeable ghosts and inside-out vesicles from human erythrocyte membranes. *Methods Enzymol. 31* 172–180.

(145) Brähler, M., Georgieva, R., Buske, N., Müller, A., Müller, S., Pinkernelle, J., Teichgräber, U., Voigt, A., and Bäumler, H. (2006) Magnetite-Loaded Carrier Erythrocytes as Contrast Agents for Magnetic Resonance Imaging. *Nano Lett. 6*, 2505–2509.

(146) Yoo, J.-W., Irvine, D. J., Discher, D. E., and Mitragotri, S. (2011) Bio-inspired, bioengineered and biomimetic drug delivery carriers. *Nat. Rev. Drug Discov. 10*, 521–535.

(147) Antonelli, A., Sfara, C., Battistelli, S., Canonico, B., Arcangeletti, M., Manuali, E., Salamida, S., Papa, S., and Magnani, M. (2013) New Strategies to Prolong the In Vivo Life Span of Iron-Based Contrast Agents for MRI. *PLoS ONE*, 1-17.

(148) Sherry, A. D., and Woods, M. (2008) Chemical Exchange Saturation Transfer Contrast Agents for Magnetic Resonance Imaging. *Annu. Rev. Biomed. Eng.* *10*, 391–411.

(149) Haavik, J., Martínez, A., Olafsdottir, S., Mallet, J., and Flatmark, T. (1992) The incorporation of divalent metal ions into recombinant human tyrosine hydroxylase apoenzymes studied by intrinsic fluorescence and 1H-NMR spectroscopy. *Eur. J. Biochem.* *210*, 23–31.

(150) Olafsdottir, S., and Martínez, A. (1999) The Accessibility of Iron at the Active Site of Recombinant Human Phenylalanine Hydroxylase to Water As Studied by 1H NMR Paramagnetic Relaxation. *J. Biol. Chem.* *274*, 6280–6284.

(151) Zoidakis, J., Loaiza, A., Vu, K., and Abu-Omar, M. M. (2005) Effect of temperature, pH, and metals on the stability and activity of phenylalanine hydroxylase from Chromobacterium violaceum. *J. Inorg. Biochem.* *99*, 771–775.

(152) Loaiza, A., Armstrong, K. M., Baker, B. M., and Abu-Omar, M. M. (2008) Kinetics of Thermal Unfolding of Phenylalanine Hydroxylase Variants Containing Different Metal Cofactors (Fe$^{II}$, Co$^{II}$, and Zn$^{II}$) and Their Isokinetic Relationship. *Inorg. Chem.* *47*, 4877–4883.

(153) Hartley, M. D., Larkin, A., and Imperiali, B. (2008) Chemoenzymatic synthesis of polyprenyl phosphates. *Bioorg. Med. Chem.* *16*, 5149–5156.

# 6    Appendix A – Methods for screening metal binding in phenylalanine hydroxylase

## Background and motivation

One of the objectives of the thesis was to engineer a high relaxivity metalloprotein as a higher signal contrast agent necessitates less material to be used during imaging. Phenylalanine hydroxylase (PAH) was selected as the scaffold protein for engineering as it is a native metalloprotein that binds a non-heme iron with catecholamine dissociation constants reported over a large range, from nanomolar to submillimolar.[130–132] Crystal structures show displacement of two iron-coordinated water molecules due to catecholamine binding[134] and there have been reports of relaxivity change upon binding of millimolar concentrations of ligand.[149,150] PAH has also shown affinity for other metals and low specificity for iron *in vitro*,[151,152] suggesting flexibility in the metal binding site.

We sought to redesign the PAH metal binding pocket such that the protein has higher binding affinity for gadolinium. Gadolinium has the most unpaired electrons of any ion and is thus theoretically able to generate the highest MRI signal.[4] An approach for obtaining a lanthanide-binding PAH mutant would be through directed evolution, which involves rounds of random mutagenesis and screening to optimize the protein for a desired property.[19] The success of implementing directed evolution is dependent on having an effective screen. Below I will discuss a terbium fluorescence based screen that was investigated and its compatibility with library screening.

**Results and discussion**

Of the lanthanides, terbium exhibits luminescence when it is bound to a protein and in close proximity to aromatic amino acid residues such as tryptophan, tyrosine, or phenylalanine. This property has been used to analyze protein structure, protein-ligand and protein-protein interactions, particularly through the use of a class of peptides known as lanthanide-ion binding tags (LBTs).[125] We assessed the feasibility of using terbium luminescence as a read out of lanthanide binding affinity of PAH since has two tryptophan residues near the metal binding site.[135]

Titrations of increasing concentrations of terbium onto apo-PAH resulted in an increase in fluoresnce emission at 540 nm, which produced a sigmoidal binding curve when plotted against terbium concentration (Figure A1). Fitting of one site binding to this data gave a terbium dissociation constant $K_d$ of 78 μM for wild type PAH. The fluorescence read out makes this assay adaptable for use with a plate reader. However, since luminescence resonance energy transfer (LRET) between terbium and the protein is dependent on the presence of tryptophan residues, this assay may give spurious results for library mutants that substitute the tryptophan residues.

We also investigated whether the terbium signal could be used to probe dopamine binding. We hypothesized that binding of dopamine would interfere with the LRET between terbium and the tryptophan residues, resulting in a decrease in signal that could be used to quantify the dopamine binding affinity. However, our experiments show a different effect whereby fluorescence emission increases with dopamine concentrations up to approximately 1

mM before decreasing (Figure A2). Perhaps there is signal enhancement from the aromatic ring of dopamine.

We tested the application of this assay in screening in 96-well plate format with a PAH library of 24 mutants generated by random mutagenesis. The mutants were expressed in E. coli with an N-terminal 6xHis tag and purified in parallel in a filter bottom 96-well plate and exchanged into hepes buffer using a pre-packed desalting plate. Terbium was added in small increments and the fluorescence emission was read for each addition to obtain a binding curve for each mutant. The results indicated variability across the screen (Figure A3). Wild type PAH was used in triplicate as a positive control and only two of the three showed similar results. Additionally, all of the library wells showed different maximum fluorescence emissions compared to WT. Sequencing of a sample of the library did not show any mutations. The signal variability may be due to differences in protein concentration across wells. Accounting for the protein concentration differences in $K_d$ equation fitting still resulted in false positives using the screen. Impurities in the purified protein could also be affecting the fluorescence readings. Lanthanides are known to bind non-specifically to various cell components, such as other proteins and DNA. Lanthanides have been used to probe protein expression in crudes, though this was used with a high affinity LBT (nanomolar $K_d$) and low terbium concentrations.[153] Our assay required up to 1 mM terbium in order to obtain a binding curve, which is likely to result in more non-specific binding with any contaminating components. The protein also precipitated at the highest concentrations of terbium used. These results indicate that in order for terbium to be used as a screen, the binding affinities of the protein need to be drastically higher than that of wild type.

## Future directions

The use of terbium for probing lanthanide binding sites is more suitable for a protein with lower $K_d$ for terbium. A different protein could be used as the starting scaffold or PAH can be tuned using rational or semi-rational design to have lower $K_d$ for terbium before being used for library construction by random mutagenesis. Additionally, the purification of the library may require optimization in order to obtain uniform protein concentration and minimize the number of false positives using the screen. Since the goal is to obtain a high relaxivity protein, high terbium affinity mutants isolated from each round should be tested by MRI before proceeding with further evolution rounds.

## Methods and materials

### PAH mutant library construction

PAH mutant libraries were generated by random mutagenesis of the open reading frame. Mutations were introduced through error prone PCR using the DNA polymerase Mutazyme II from the GeneMorph II Random Mutagenesis Kit (Agilent). To achieve 1-2 amino acid changes, we used 400 ng of template and 30 PCR cycles. PCR was set up according to the manufacturer protocols. The mutated gene was used as primers for inverse PCR using the parent wild type PAH vector as the backbone and the high fidelity DNA polymerase Phusion (New England Biolabs). After cycling, the reaction was treated with the restriction enzyme *Dpn* I to digest the parental DNA. The remaining synthesized PCR product was transformed into XL Gold *E. coli* cells and plated onto agar with 50 µg/mL kanamycin.

## PAH library expression

Colonies picked from the library were grown in deep well (2.7 mL/well) square, 96-well plates in 1.5 mL working volume of M9 minimal media. The plate was covered with a gas permeable plate seal and incubated at 37°C, 500 rpm on a 3 mm orbital shaking incubator overnight. These overnight cultures were used to seed the expression cultures in square, 24-well plates (6 mL/well), with 4 mL working volume and 1 mL of overnight culture as inoculant. The plates were again covered with gas permeable seals and incubated at 37°C and 100-150 rpm in the floor shaking incubator for 4 h when the OD600 should reach approximately 0.8-1.0. 5 μL of 1 mM IPTG was added to each well and the plate was returned to the incubator for an additional 5 h. After expression, the plate was centrifuged at 3000 x g for 20 min to pellet the cultures. The supernatant was removed and pellets stored at -80°C until purification.

## 96-well format protein purification

To each well/pellet, 250 μL of Bugbuster mixed with lysonase and EDTA-free protease inhibitor cocktail (EMD Millipore) was added. The pellets were incubated with the mixture for 20 min with shaking at room temperature to lyse the pellets. The lysate was then transferred to a filter bottom 96-well plate (Pall). The filter plate was stacked on top of a collection plate and centrifuged together at 1500 x g until all of the filtrate has been collected. The soluble lysate was then transferred to another filter bottom 96-well plate and 100 μL of 50% Ni-NTA slurry (Qiagen) was added to each well. A collection plate was placed underneath the filter plate to catch any leaking. The two plates were shaken together for 2 h in the cold room (4°C). The plates were then centrifuged at 1500 x g for 5 min to remove the lysate. Each well was washed with 300 μL of Ni-NTA wash buffer 6 times. To elute the protein, a clean collection plate was placed

under the filter plate and 120 µL of elution buffer was added to each well. The plate was shaken with the elution buffer for 10 min, then centrifuged at 1500 x g for 5 min to collect the eluted protein. The eluted protein was desalted over a pre-packed desalting plate (GE Life Sciences) that had been equilibrated with 50 mM hepes 150 mM KCl pH 7.4 buffer.

## Protein quantification

The concentration of the purified protein was determined used the Pierce 660 protein assay with an undiluted sample and a 1:2 dilution sample of protein from each well following the product information. Bovine serum albumin was used as the standard.

## Terbium titration for protein library

Based on the protein concentrations determined using the Pierce 660 assay, the protein was diluted to approximately 1-5 µM. The protein was transferred to a clear bottom black 96-well plate. Each well had 100 µL of protein. $TbCl_3$ solutions of various concentrations were prepared fresh in $ddH_2O$. Lanthanide solutions were added to each well in progressively increasing concentrations, reading the fluorescence of the plate between additions. The fluorescence emission spectra were read from 500 nm to 600 nm with excitation at 276 nm.
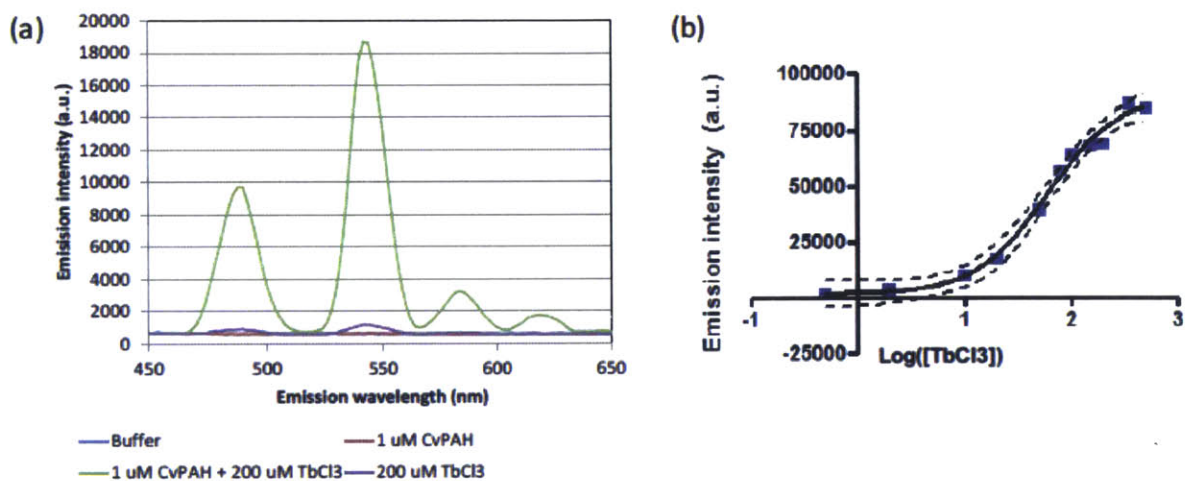
**Figure A1.** (a) Titration of increasing concentrations of $TbCl_3$ onto wild type PAH results in a fluorescence emission increase at 540 nm with excitation at 276 nm. (b) Terbium $K_d$ of wild type PAH was found to be 78 μM from the peak emission at 540 nm.
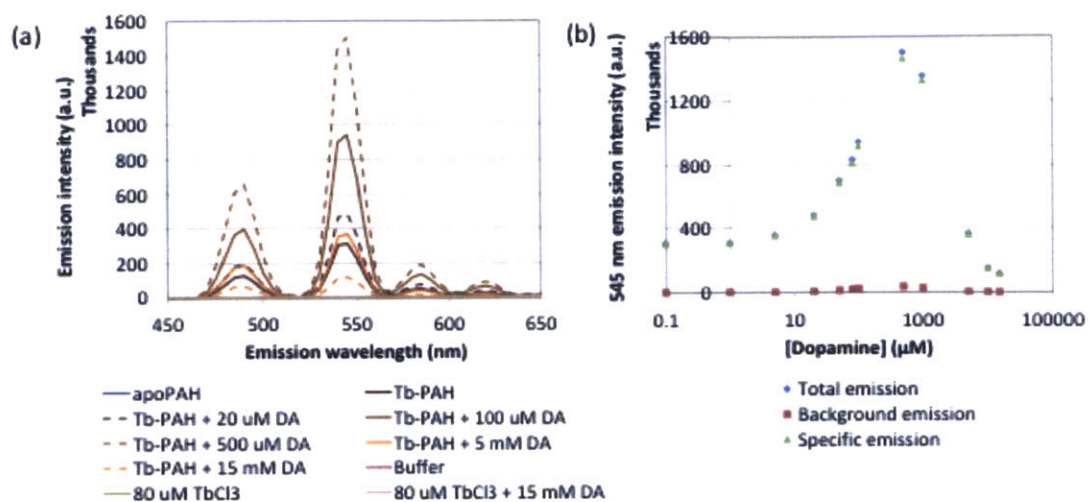
(a) legend:
— apoPAH
- - Tb-PAH + 20 uM DA
- - Tb-PAH + 500 uM DA
- - Tb-PAH + 15 mM DA
— 80 uM TbCl3

— Tb-PAH
— Tb-PAH + 100 uM DA
— Tb-PAH + 5 mM DA
— Buffer
— 80 uM TbCl3 + 15 mM DA

(b) legend:
• Total emission
■ Background emission
▲ Specific emission

**Figure A2.** (a) Addition of dopamine to $Tb^{3+}$-PAH (wild type) first increases the peak emission at 540 nm followed by decreases at concentrations above 1 mM. (b) The behavior of the emission results in an incomplete binding curve for dopamine titration onto $Tb^{3+}$-PAH. Background emission is the emission from $TbCl_3$ solutions with the indicated concentrations of dopamine.
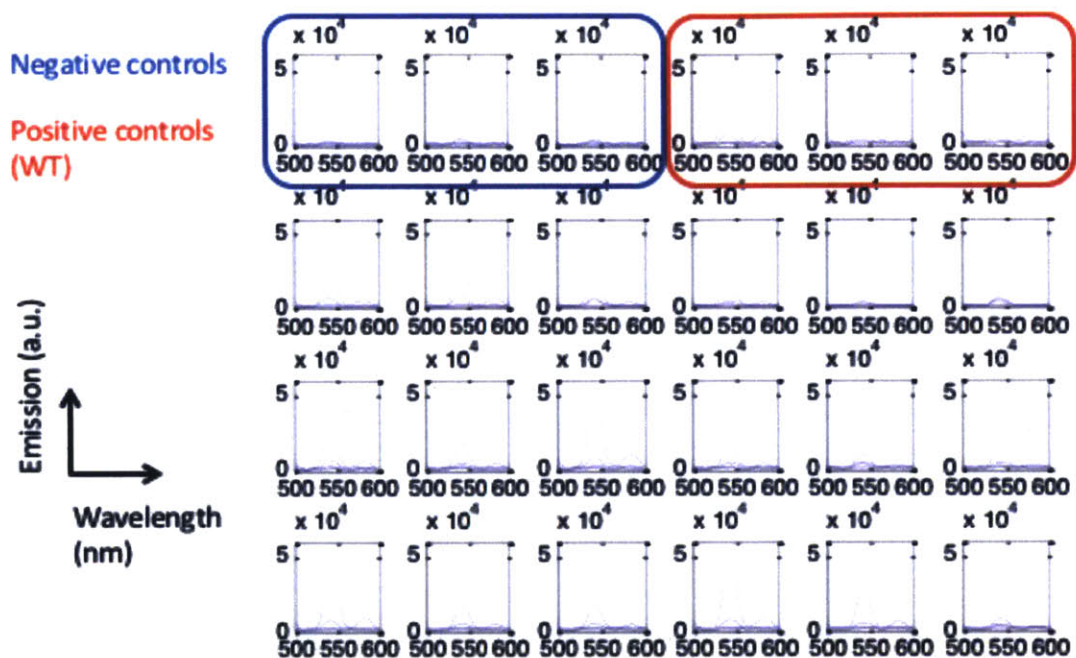
**Figure A3.** Emission spectra from terbium titrations onto a sample PAH mutant library show variability in fluorescence. Each subplot shows the titration spectra from one well of a 96-well plate, with each well representing one colony picked from the library. Negative control contains buffer without any protein. Positive control contains wild type PAH.